



## ORIGINS OF BLADE-LIKE DIKES IN VOLCANIC RIFT ZONES

By Allan M. Rubin<sup>1</sup> and David D. Pollard<sup>2</sup>

### ABSTRACT

Seismic and geodetic data have demonstrated that dikes in the rift zones of Kilauea Volcano in Hawaii and Krafla Volcano in Iceland are typically intruded laterally from a central magma reservoir and acquire a blade-like form. A remarkable feature of many such dikes is that they propagate at shallow depths for tens of kilometers without erupting. Using concepts of fracture mechanics, we can specify the conditions necessary for this type of growth. A dike will propagate if the stress-intensity factor at the dike tip exceeds a critical value, known as the fracture toughness of the host rock. An increase in the rift-zone fracture toughness with depth could limit the depth to which dikes extend, but little existing evidence supports this possibility. We find that several geological processes could contribute to a distribution of the stress-intensity factor along the dike perimeter that would promote the development of a blade-like form.

Factors influencing the stress intensity along the dike perimeter can be divided into two categories: factors pertaining to the dike geometry, including the dike size, shape, and depth beneath the Earth's surface; and factors pertaining to the distribution of driving pressure (magma pressure minus the remote stress) acting on the dike plane. The pressure within the dike is controlled by magma-reservoir pressure, magma density, presence of vesiculated magma or gas at the dike top, and pressure gradients due to viscous flow. Possible contributors to the remote stress include density stratification of the rift zone, gravitational loading of the volcanic ridge, intrusion of previous dikes, faulting, and plate tectonic forces.

Of the geometric factors, both the elongate dike shape and the proximity of the Earth's surface tend to promote upward growth and eruption, rather than continued lateral growth of the dike. Thus a blade-like form must be the result of a driving-pressure distribution that increases the stress-intensity factor at the downrift edge of the dike with respect to that at the dike top and bottom. This can be achieved if the driving pressure is greater at the depth of the dike center than at the dike top or bottom. The vertical pressure variation within a laterally propagating dike is essentially equal to that within a static body of magma. The presence of vesiculated magma in the upper part of the dike enhances upward propagation but has little effect on downward and lateral propagation. Thus the source of the greater driving pressure at the depth of the dike center must be the remote stress; each of the contributors to this stress listed above is a potential source of such a stress distribution.

Using the cross-sectional geometry of the August 1981 southwest-rift-zone dike at Kilauea inferred from geodetic data, and assuming a uniform fracture toughness within the rift zone,

we estimate the magma pressure and the remote stress at the time of intrusion. The hydrostatic head of the magma was deeper than 50 m below the surface. The excess magma pressure at the dike center was 2.5–10.5 MPa (25–105 bars), and the driving pressure decreased toward the dike top and bottom by about 3–11 MPa/km. If the gradients in the driving pressure toward the dike top and bottom were due only to the local density contrast between the magma and the host rock, they would be about 3 MPa/km. A more precise determination of the driving pressure is not possible without more precise values of the rift-zone fracture toughness and elastic shear modulus. From estimates of the dike thickness, we find that the rift-zone shear modulus is within a factor of 2–3 of 3 GPa. This is in agreement with other in-place determinations of the shear modulus and about an order of magnitude less than laboratory values for intact basalt.

### INTRODUCTION

Geological studies of eroded Hawaiian and Icelandic volcanoes have documented the importance of shallow dike intrusion as a mechanism of magma transport in these distinct geologic settings. The majority of such dikes are nearly vertical and occur within swarms, or rift zones, that may be more than 100 km long and contain hundreds or thousands of dikes (Walker, chapter 41; Macdonald, 1956; Walker, 1959; Walker, 1963; Fiske and Jackson, 1972; Helgason and Zentilli, 1985). During the last few decades, abundant geological, geochemical, petrological, geophysical, and geodetic data collected from Kilauea and Mauna Loa by scientists at the Hawaiian Volcano Observatory and from Krafla by scientists at the National Energy Authority and the Nordic Volcanological Institute in Iceland have shed considerable light on some of the processes of magma movement and dike emplacement. At both locations, rapid subsidence of the region overlying a shallow magma reservoir is associated with the lateral flow of magma for up to several tens of kilometers into adjacent rift zones. In most cases, this intrusion of magma results in the formation of new dikes, the surface manifestations of which may include observable rift-zone widening and fissure eruptions. The 120-km-long east rift zone of Kilauea, and historical and prehistoric dikes in Iceland that vented nearly 100 km from their sources (Sigurdsson

<sup>1</sup>Department of Geology, Stanford University, Stanford, CA 94305.

<sup>2</sup>Departments of Geology and Applied Earth Sciences, Stanford University, Stanford, CA 94305.

and Sparks, 1978), attest to the extraordinarily extensive form rift-zone dikes can take.

Dikes propagate because the magma pressure within them fractures the rock ahead of the magma front or forces preexisting fractures, such as cooling joints or through-going rift-zone extension cracks, to widen. In either case, this propagation can be interpreted in terms of established principles of fracture mechanics (see, for example, Lawn and Wilshaw, 1975). If the resistance of the host rock to fracture, the magma pressure within the dike, and the remote stress acting perpendicular to the rift zone are known, the directions in which the dike will propagate can be predicted. Alternatively, observations of dike propagation can be used to estimate some of these parameters.

We first summarize the available evidence on dike geometry and emplacement and outline the theoretical model to be used. We then list and analyze the factors governing the horizontal and vertical propagation of basaltic dikes emanating from near-surface magma reservoirs. Using this analysis we estimate the magma pressure and the state of stress in the southwest rift zone at Kilauea for the August 1981 dike intrusion. The model provides a framework for discussion of rift-zone dynamics and possible future research.

#### ACKNOWLEDGMENTS

This paper benefited from careful reviews by Paul Delaney, Kieth Evans, Steve Martel, Larry Mastin, Michael Ryan, and Hans Weertman. Paul Davis, Bob Decker, Jim Dieterich, John Dvorak, David Hill, and Fred Klein provided interesting discussions and early versions of some results. We thank John Dvorak, Jack Lockwood, and Arnold Okamura for a kind introduction to Hawaii Volcanoes National Park and the Hawaiian Volcano Observatory. This research was funded in part by a National Science Foundation Graduate Fellowship and NSF grant EAR-8520641.

### CHARACTERIZATION OF THE DIKE- EMPLACEMENT PROCESS

#### OBSERVATIONS OF DIKE PROPAGATION AND GEOMETRY

Combined geodetic and seismic data have revealed the presence of a magma chamber or chambers at approximately 2–7 km below the surface at Kilauea, Mauna Loa, and Krafla Volcanoes. During periods of activity these magma chambers inflate slowly, at rates of a few cubic meters per second, over periods of months or years, and deflate rapidly, at rates of 100–1,000 cubic meters per second, for periods of several hours to a few days. Typically, summit subsidence is accompanied by swarms of shallow earthquakes that migrate downrift at velocities of a few tens of centimeters per second (Klein and others, chapter 43; Brandsdottir and Einarsson, 1979). These swarms sweep out tabular zones that are typically 1–2 km wide, a few kilometers high, and as much as several tens of kilometers long. Ground cracking or fissure eruptions may shortly precede or follow the migration of the earthquake swarm beneath a particular site (Hauksson, 1983; F.W. Klein, oral commun.,

1985). Deviations from this simple pattern are not, however, uncommon during intrusions into the east rift zone (ERZ) of Kilauea: there some earthquake swarms originate within the rift zone itself, and discontinuous or uplift migration of earthquakes is sometimes observed (Klein and others, chapter 43).

Although the factors controlling the origin and extent of the earthquake swarms are not yet understood, it seems reasonable to use these earthquakes to estimate dike location (Brandsdottir and Einarsson, 1979; Ryan and others, 1981). The approximate boundaries of earthquake swarms associated with a few well-documented intrusions at Kilauea and Krafla are shown on figure 53.1, projected onto cross sections parallel to the rift axes.

Pollard and others (1983) derived a graphical method for estimating the height, depth, dip, and thickness of dikes from surface vertical-deformation data. Although geodetic data are available less frequently than earthquake-source data, their interpretation may improve dike location accuracy considerably. Displacements measured in the rift zones of Kilauea and Krafla yield dike heights and depths consistent with estimates from earthquake-source data. Estimates of dike thickness (0.8–2 m) and of dike dip (within a few degrees of vertical) are both in agreement with observations of eroded rift-zone dikes.

#### THEORETICAL CONSTRAINTS ON DIKE STABILITY AND PROPAGATION

In this study dikes are represented as pressurized cracks in an isotropic, homogeneous, linearly elastic half-space. Field observations indicate that dikes are typically nearly planar features. Although the assumptions of isotropy, homogeneity, and elasticity are certainly incorrect in detail (Ryan and others, 1983), we believe the model is appropriate for the physical insight sought here. Geodetic measurements made during the current Puu Oo activity show that rift-zone extension accumulated prior to an eruptive phase is completely recovered following eruption. This indicates that the volcano is capable of elastic behavior over periods of weeks and distances of a few kilometers (Hoffman and others, 1984).

It has been well established theoretically and experimentally that a crack will propagate if the energy available, from work done on the system by the boundary forces (remote stress and magma pressure) and from any release of stored strain energy in the surrounding solid, is sufficient to supply the energy expended in the cracking process (Lawn and Wilshaw, 1975). Though the solid is assumed to be elastic, the theory is sufficiently general that it incorporates inelastic behavior (such as secondary fracturing or local plastic deformation) in a small region around the crack tip. This region is called the process zone.

Another crack propagation criterion, equivalent to the above energy-balance criterion, involves the use of quantities known as stress-intensity factors (Lawn and Wilshaw, 1975). A dilated crack in an elastic material generates stresses in the near-tip region given by

$$\sigma_{ij} = K f_{ij}(\theta)/(2r)^{1/2} \quad (1)$$

where  $\sigma_{ij}$  are components of the stress tensor,  $K$  is the mode I (tensile) stress-intensity factor,  $r$  is the distance from the crack tip,

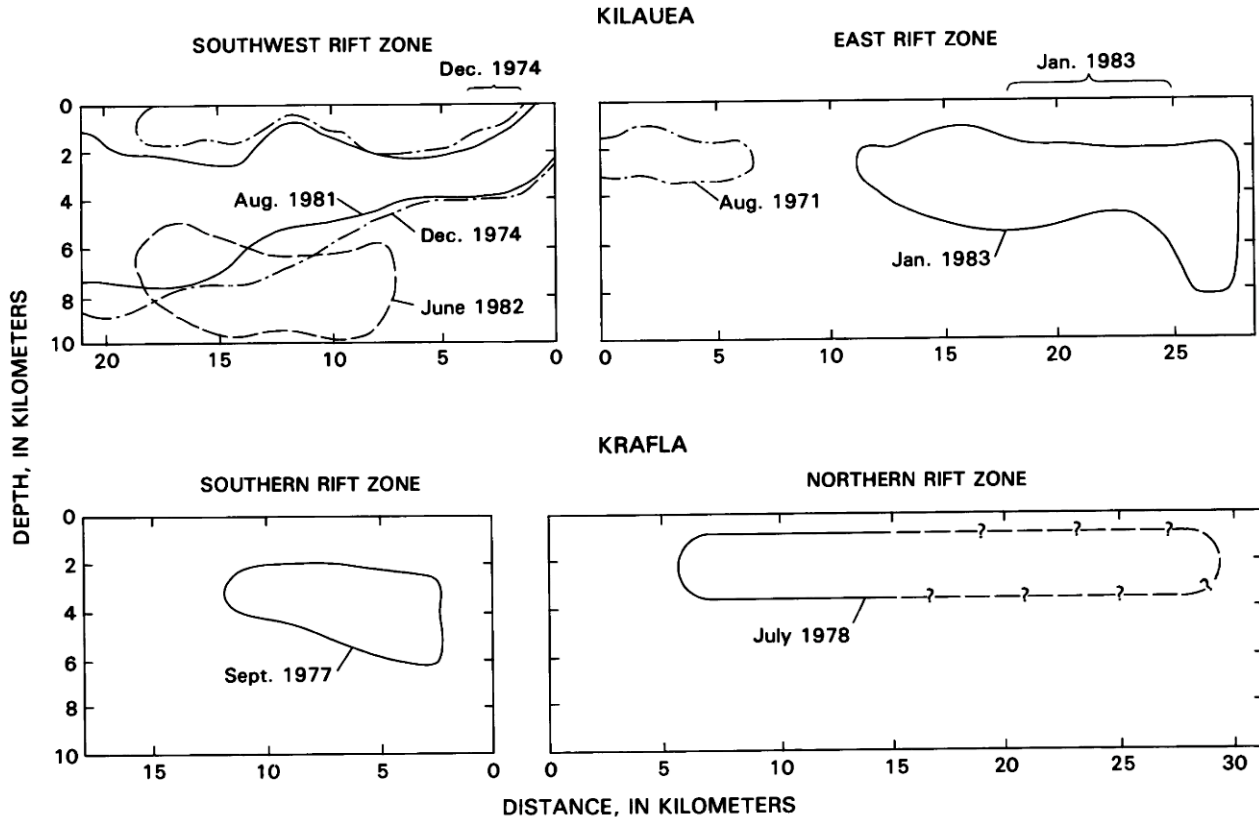


FIGURE 53.1.—Approximate limits of seismic swarms associated with some well-documented dike intrusions at Kilauea and Krafla Volcanoes, projected onto cross sections parallel to the rift axes. The origins for the distance axes are near Halemaumau Crater within the summit caldera at Kilauea and at the center of the caldera at Krafla. Extent of associated eruptive fissures indicated by brackets at the tops of the sections. Note the apparent lack of seismicity, due in part to the low-magnitude filter applied to the data, near the eruption site of the 1983 east-rift-zone intrusion at Kilauea. Data for Kilauea from Klein and others (chapter 43); data for Krafla from Brandsdottir and Einarsson (1979) and Einarsson and Brandsdottir (1979).

and the  $f_{ij}(\theta)$  are functions of position around the crack tip (fig. 53.2). (By an alternate convention, this equation would contain an additional factor of  $\pi^{-1/2}$ , and the value of  $K$  would be modified accordingly.)  $K$  is in general dependent only upon the crack geometry and the distribution of driving pressure  $\Delta P$ . We consider the driving pressure for dikes to be a function of vertical position  $y$ : it is equal to the magma pressure  $P_m(y)$  minus the remote stress  $S(y)$  acting perpendicular to the dike plane:

$$\Delta P(y) = P_m(y) - S(y). \quad (2)$$

A dike will propagate if its stress-intensity factor is greater than a critical value  $K_c$ , termed the fracture toughness of the rock.<sup>1</sup> A

negative value of  $K$  indicates that a dike will decrease in length by pinching shut at its tip. A dike is stable if  $0 < K < K_c$ ; that is, the dike will neither increase nor decrease in length (Weertman, 1971).

For dikes following preexisting fractures, as is possible in volcanic rift zones,  $K_c$  could be zero. Experimentally determined values of  $K_c$  for intact laboratory specimens of basalt at room temperature and pressure lie within the range  $1\text{--}2 \text{ MPa} \cdot \text{m}^{1/2}$  (Atkinson, 1984). However, estimates of  $K_c$  from studies of dikes exposed in shale (Delaney and Pollard, 1981), made under the assumption that magma had access to the dike tip, are in the range  $30\text{--}100 \text{ MPa} \cdot \text{m}^{1/2}$ . Examination of dike-parallel joints in sandstone (Delaney and others, in press) suggests that the crack tip process zone associated with propagating basaltic dikes can be

<sup>1</sup>Because crack propagation can proceed much more rapidly than magma flow, it is expected that in actuality  $K$  will exceed  $K_c$  by only an infinitesimal amount. Physically this may be accomplished by the opening of a low-pressure cavity at the dike tip. The action of the remote compressive stress on this cavity would decrease  $K$  to values below that calculated assuming that magma had access to the dike tip. In subsequent calculations of  $K$  we assume that magma has access to the dike tip, and interpret a value of  $K$  greater than  $K_c$  as indicating that propagation will proceed.

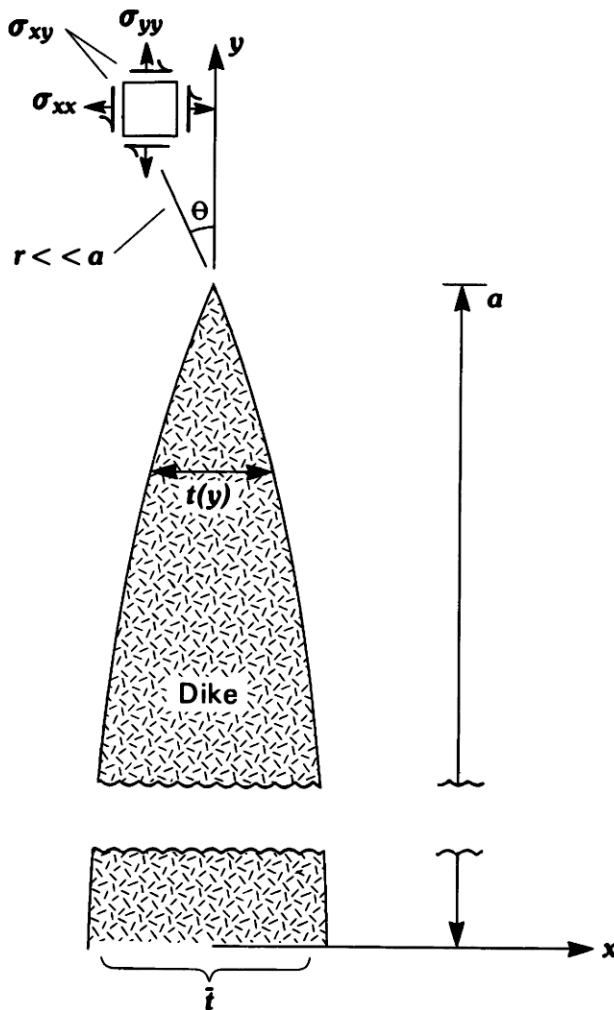


FIGURE 53.2.—Stresses ( $\sigma$ ) in the near-tip region of a crack or dike. The stress is a function of the distance  $r$  from the dike tip, the position  $\theta$  around the dike tip, and the stress-intensity factor  $K$  (eq 1).  $a$ , dike half-length;  $t(y)$ , dike thickness at a height  $y$  above the dike center;  $\bar{t}$ , average dike thickness.

larger than that associated with cracks in laboratory specimens, giving larger values of  $K_c$ . Frictional sliding on fractures near the dike, which is indicated by rift-zone earthquake swarms, is another energy-expending mechanism that would increase  $K_c$ .

The effects of pressure and temperature on  $K_c$  are at present only poorly understood. For dry rock (Schmidt and Huddle, 1977; Winter, 1983)  $K_c$  increases with increasing pressure because the added confining pressure inhibits microcracks near the crack tip from opening up and aiding propagation (Atkinson, 1984). When these microcracks are accessible to fluids at pressures equal to the confining pressure, for example in experiments on water-saturated sandstone (Winter, 1983), this effect is not apparent. For moderate temperatures, increasing temperature decreases  $K_c$  because the energy

required for brittle fracture is reduced. Limited experimental determinations indicate that  $K_c$  for gabbro decreases by about 30–35 percent from room temperature to 400°C (Meredith and Atkinson, 1985). At some higher temperature, increased plasticity at the crack tip will cause  $K_c$  to increase. Bjornsson (1985) estimates the temperature at 4–5 km depth in Icelandic rift zones to be 500–600°C. Although more experimental data are needed, we assume these temperatures to be low enough that increased crack-tip plasticity is not a significant factor at the time-scales appropriate for dike intrusion.

Because of sparse high-temperature and high-pressure data, and because of the possible discrepancy between values of  $K_c$  appropriate for cracks in laboratory specimens and for dikes in the Earth's crust, we can only restrict the probable range of critical stress-intensity factors to

$$0 > K_c > 100 \text{ MPa} \cdot \text{m}^{1/2}.$$

#### THEORETICAL CONSTRAINTS ON DIKE THICKNESS

The length-to-height ratio of typical rift-zone dikes justifies treating them as two-dimensional when calculating dike thickness. For a uniform driving pressure  $P_o$ , the thickness of the dike at a distance  $y$  from its center is given by Pollard and others (1983) as:

$$t = P_o a \frac{(1 - \nu)}{\mu} [1 - (y/a)^2]^{1/2} \quad (3)$$

(fig. 53.2), where  $a$  is the dike half-height,  $\nu$  is Poisson's ratio, and  $\mu$  is the elastic shear modulus. The average dike thickness,  $\bar{t}$ , is about 0.8 times the thickness at the dike center. Equation 3 illustrates the general relation that dike thickness is proportional to dike half-height and driving pressure, and inversely proportional to rock stiffness,  $\mu/(1 - \nu)$ .

Given estimates of the dike thickness-to-height ratio from geodetic data, one can calculate the ratio of driving pressure to rock stiffness. If the rock stiffness is known, one can then estimate the driving pressure. Experimentally determined values of  $\nu$  for basalt vary only slightly, generally lying between 0.22 and 0.28 for conditions ranging from room temperature and pressure to those appropriate for depths of several kilometers (Birch, 1966; Ryan and others, 1983). Typical static laboratory values of  $\mu$  for basalt are 25–35 GPa (Birch, 1966). However, the shear moduli determined from loading large fractured rock masses in the field are lower than those measured on pristine samples in the laboratory by as much as an order of magnitude (Bieniawski, 1978; Evans, 1982). In actuality the effective shear modulus of the rock mass intruded by dikes probably increases with depth as the rock becomes more competent. From the lack of a significant piezomagnetic anomaly during periods of magma-chamber inflation, Davis (1976) estimates that the effective shear modulus of the summit region of Kilauea is about an order of magnitude less than that of competent basalt. We accept this estimate as a more appropriate average shear modulus for volcanic rift zones than the laboratory value. However, the large uncertainty associated with this figure makes the dike thickness-to-height ratio only a weak constraint on the driving pressure.

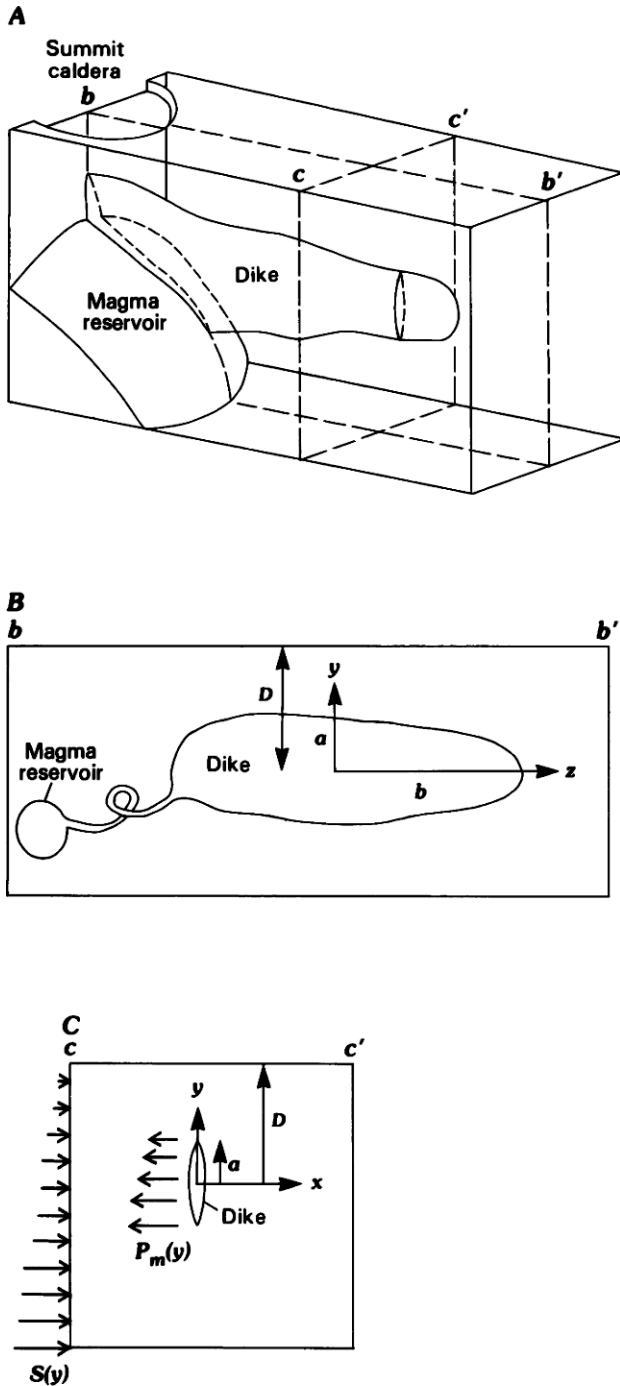


FIGURE 53.3.—Diagrams of a rift-zone dike intruded laterally from a shallow magma reservoir. *A*, Cartoon sketch of the dike showing general form; planes of sections *B* and *C* indicated. *B*, Idealized longitudinal section of the dike, which has a half-height  $a$ , a half-length  $b$ , and a depth  $D$ . The magma reservoir acts as a source of pressure. *C*, Idealized cross section of the dike. A remote stress  $S(y)$  acts perpendicular to the dike plane; a magma pressure  $P_m(y)$  acts within the dike.

#### PROPAGATION AND STABILITY CRITERIA FOR RIFT-ZONE DIKES

In most cases the region swept out by individual earthquake swarms remains fairly constant in vertical extent and depth as the magma travels great distances laterally. From this observation we infer that the dikes are adopting an approximately equilibrium position in the vertical plane; it is this inference that motivates the analysis which follows. The possibility that some kinetic factor related to magma flow or solidification inhibits dikes from reaching their stable position is considered briefly in the section "Discussion."

The necessary conditions for a dike to have a propagating downrift edge and a stable height are that  $K \geq K_c$  at the downrift edge and  $K < K_c$  at the top and bottom. These conditions can be met by increasing  $K_c$  at the dike top and bottom relative to  $K_c$  at the downrift edge, or by decreasing  $K$  at the dike top and bottom relative to  $K$  at the downrift edge. In what follows we assume a uniform value of  $K_c$  throughout the rift zone and examine the factors that could contribute to the required variation in  $K$ . We infer from the blade-like geometry of typical rift-zone dikes that during downrift propagation sections of the dike top and bottom close to the downrift edge have attained their stable height. This assumption allows us to neglect lateral magma pressure gradients due to both viscous flow and along-strike changes in dike elevation when comparing  $K$  at the downrift edge to that at the dike top and bottom.

#### FACTORS CONTROLLING DIKE PROPAGATION

A rift-zone dike intrusion is shown in cartoon form in figure 53.3A, and our idealizations of the dike to be used for modeling purposes are illustrated in figures 53.3B and 53.3C. The model dike has a half-height  $a$ , half-length  $b$ , and depth  $D$ . It is embedded in an elastic half-space with uniform shear modulus  $\mu$  and fracture toughness  $K_c$ . The magma reservoir is represented as a source of pressure located at the uprift end of the dike, but is not explicitly accounted for in calculations of  $K$ , because it is distant from the part of the dike perimeter that is of interest. The magma has a uniform viscosity  $\eta$  and a uniform or vertically varying density  $\rho_m(y)$ . A vertically varying remote stress  $S(y)$  acts on the plane of the dike, and a vertically varying magma pressure  $P_m(y)$  acts within the dike.

The geologic factors contributing to the stress intensity around the dike can be divided into two categories: those pertaining to the geometry of the dike, and those pertaining to the driving-pressure distribution. The first category includes the dike size, shape, and depth beneath the Earth's surface. The second category can be divided into those factors related to the magma or gas pressure within the dike and those factors related to the remote stresses acting perpendicular to the dike plane. The pressure distribution within the dike body is controlled by the unvesiculated magma density, the presence or absence of vesiculated magma or a separate gas phase, the time-varying magma-reservoir pressure, and pressure loss due to viscous flow. For conceptual purposes, the remote stress acting on the dike plane can be subdivided into two components: the lithostatic load or weight of the rock overburden, including variable density stratification; and any supplementary stresses induced by

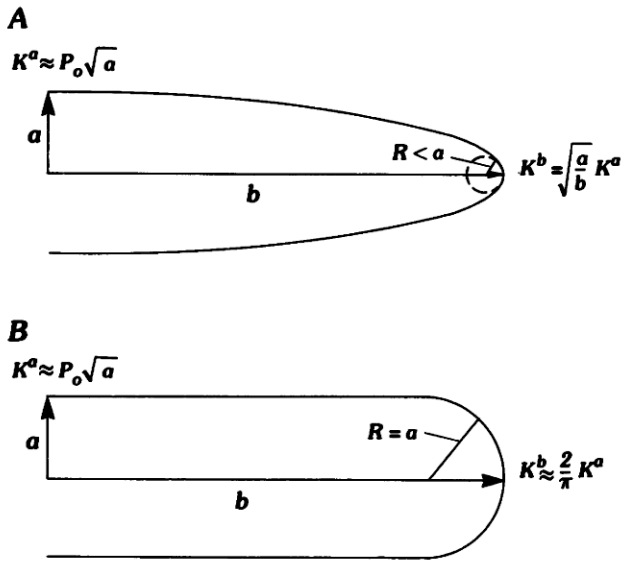


FIGURE 53.4.—Idealized longitudinal sections showing dike geometry. Dikes subject to uniform driving pressure,  $P_o$ . **A**, Elliptical dike with half-height  $a$  and half-length  $b$ . The radius of curvature  $R$  in the plane of the dike at the downrift edge is less than  $a$ ; as the dike grows laterally,  $K^b$  decreases approximately as  $\sqrt{a/b}$ . **B**, Dike with a constant half-height  $a$  except near its downrift edge, where  $R$  is equal to  $a$ . The larger radius of curvature gives rise to a larger value of  $K^b$  than for the ellipse. This idealization is used in this study and is likely to produce an overestimate of  $K^b$ .

topographic relief, slip along major faults at depth, the intrusion of earlier dikes, or plate-tectonic forces.

#### GEOMETRICAL FACTORS

##### DIKE SIZE

For a two-dimensional dike of half-height  $a$  subjected to a uniform driving pressure  $P_o$  (fig. 53.3C,  $D = \infty$ ), the stress-intensity factor at the dike top and bottom is

$$K = P_o \sqrt{a}. \quad (4)$$

This equation illustrates the general result that  $K$  is proportional to the square root of the dike half-height. For a propagating dike subject to a uniform, steady driving pressure,  $K$  increases with height, so propagation should never cease and eruptions would be inevitable.

##### DIKE SHAPE

If the dike is idealized as having an elliptical shape with half-height  $a$  and half-length  $b$  (fig. 53.4A), the stress-intensity factor around the dike perimeter can be obtained analytically. For a uniform driving pressure the stress intensity at the top or bottom of the dike is given by

$$K^a = \frac{1}{\Phi} P_o \sqrt{a} \quad (5)$$

(Broek, 1982, p. 81), where  $\Phi$  is a function of  $b/a$  that can be evaluated using tables of elliptic integrals and that approaches unity as  $b/a$  becomes large. For  $b/a = 3$ ,  $K$  is less than that for an infinitely long dike of height  $a$  by only 12 percent.

The ratio of the stress-intensity factor at the tip of the minor axis to that at the tip of the major axis is given by

$$\frac{K^a}{K^b} = \left[ \frac{b}{a} \right]^{1/2}. \quad (6)$$

Equation 6 indicates the tendency of such dikes to grow into more equidimensional forms: as the eccentricity of the ellipse increases, the stress-intensity factor at the tip of the minor axis increases with respect to that at the tip of the major axis. For rift zone dikes with  $b/a = 10$ , the ratio  $K^a/K^b$  is about 3. Because  $K^a$  for large ratios of  $b$  to  $a$  does not increase significantly if  $a$  remains constant, then equation 6 indicates that  $K^b$  actually decreases approximately in proportion to  $b^{-1/2}$ .

The dependence of  $K^a/K^b$  on  $b/a$  is in part an artifact of the assumption of ellipticity. In general, the stress intensity at a point on the perimeter of a planar crack is increased by an increase in crack size and by an increase in the in-plane radius of curvature of the crack at that point. If rift-zone dikes are constrained to maintain an elliptical shape and a fixed height, the radius of curvature at the downrift edge of the dike must decrease as the dike grows (fig. 53.4A). The decrease in  $K^b$  indicated by equation 6 shows that the effect of decreasing radius of curvature outweighs the effect of increasing crack length. If, on the other hand, the dike front approaches a semicircle of radius  $a$  (fig. 53.4B),  $K^b$  can be approximated by  $K$  for a circular crack of radius  $a$  (Paris and Sih, 1965), or

$$K^b \approx \frac{2}{\pi} P_o \sqrt{a} \quad (7)$$

(Broek, 1982, p. 81). In this case the ratio of stress-intensity factors is not very sensitive to dike length and is approximated by

$$\frac{K^a}{K^b} \approx \frac{\pi}{2}. \quad (8)$$

The actual shape of the advancing front of rift-zone dikes is unknown and will depend upon the driving-pressure distribution. In the gelatin experiments of Fiske and Jackson (1972, fig. 6), the fronts of the model dikes were somewhat elliptical. This is the expected shape for driving pressures that are greater at the depth of the dike center than at the top or bottom. We assume that the end of the dike is a semicircle of radius  $a$ . Given the likelihood of a driving pressure that is greater at the depth of the dike center (see below), and therefore a somewhat elliptical dike end, this approximation is likely to produce a slight overestimate of  $K^b$ .

## PROXIMITY OF THE EARTH'S SURFACE

The stress-intensity factors at the top ( $K^{+a}$ ) and bottom ( $K^{-a}$ ) of a two-dimensional vertical dike near a horizontal free surface and subject to a uniform driving pressure are plotted as a function of  $a/D$  in figure 53.5. The values of  $K$  are normalized to their values in an infinite body. The dike intersects the surface when  $a/D = 1$ . It can be seen that the presence of a free surface increases both  $K^{+a}$  and  $K^{-a}$ , but affects the upper dike tip more. For  $a/D < 0.5$ , the effect of the free surface becomes negligible, so  $K^{+a}$  and  $K^{-a}$  approach  $K$  for a crack in an infinite body. Shah and Kobayashi (1973) determined the stress-intensity factors around three-dimensional elliptical cracks near a free surface. Their work shows that the two-dimensional approximation is fairly good when  $a/b < 0.2$ . For all values of  $a/D$  and  $a/b$ , the free surface increases  $K^b$  by less than both  $K^{+a}$  and  $K^{-a}$ . The shaded area at the base of figure 53.5 shows the range of increase in  $K^b$  due to the free surface for various elliptical shapes. Thus the effect of the free surface on typical rift-zone dikes is to increase  $K^{+a}$ , and to a lesser extent  $K^{-a}$ , relative to  $K^b$ . That is, the surface will tend to cause the dike to increase in its vertical dimension relative to its horizontal dimension, and should enhance eruption rather than downrift propagation.

## MAGMA-PRESSURE DISTRIBUTION

Both the blade-like shape and the shallow depth of rift-zone dikes lead to stress intensities that are higher at the dike top and bottom than at its downrift edge, for uniform applied loads. If the fracture toughness of the host rock is uniform, then the observed propagation of rift-zone dikes dictates that the driving-pressure distribution must increase  $K$  at the downrift edge relative to  $K$  at the top and bottom to an extent sufficient to overcome these geometric effects. Driving-pressure distributions on vertical sections which would accomplish this are depicted schematically in figure 53.6. In these illustrations lesser excess magma pressure, or even magma underpressure, at the dike top and bottom might ensure that  $K^a < K_c$ , while the greater excess magma pressure at the downrift edge yields  $K^b \geq K_c$ . In the following sections we explore the factors governing the magma pressure within the dike. The magma pressure at any point within a dike connected to a magma reservoir is controlled by the pressure at a given point within the reservoir, the elevation of the point within the dike with respect to that point within the reservoir, the magma density, and the pressure drop due to viscous magma flow between the two points.

## MAGMA RESERVOIR PRESSURE

The occurrence of eruptions at the summit of Mauna Loa simultaneous with quiescence in the lava lake at Kilauea 3 km below precludes the existence of an open magmatic conduit from the two volcanoes' reservoirs to a common source region (Williams and McBirney, 1979). We suggest that magma rises through the crust within isolated packets to levels where it is gravitationally stable. Gravity and seismic modeling of Hawaii (Hill and Zucca, chapter 37; Broyles and others, 1979; Zucca and others, 1982) and

Iceland (Palmason, 1971) indicate that the bulk crustal density within a few kilometers of the surface is less than that of unvesiculated magma, whereas the density below is greater than that of magma. This provides an explanation for the presence of long-lived magma chambers at 2–7 km depth in Kilauea, Mauna Loa, and Krafla Volcanoes.

The magma-reservoir pressure cannot exceed that required to fracture the reservoir wall or that generated by the injection of magma from depth. However, our knowledge of the reservoir inflation and failure processes is insufficient to use them to calculate an upper bound for the reservoir pressure. We show below that dike behavior can place an upper bound on the magma-reservoir pressure. To estimate a lower bound for the reservoir pressure, we assume that the hydrostatic head of the reservoir is equal to or greater than the weight per unit area of the rock that caps it. Using densities of  $2.3 \times 10^3 \text{ kg/m}^3$  for the rock (Zucca and others, 1982) and  $2.6 \times 10^3 \text{ kg/m}^3$  for the magma (Fujii and Kushiro, 1977), we calculate hydrostatic heads of 230–350 m beneath the ground surface for reservoir tops 2–3 km deep. In an example to follow we use the more conservative estimate of –350 m as a lower bound on the hydrostatic head of the reservoir.

The change in reservoir pressure during a single dike intrusion can also affect dike behavior. If the host rock surrounding the magma chamber behaves elastically, then measured surface displacements above the chamber are proportional to pressure changes within it. Epp and others (1983) point out the linear correlation between summit tilt and vent elevation for ERZ eruptions since 1955 at Kilauea. Decker and others (1983) use this correlation to convert changes in summit tilt into differences in magma-reservoir pressure, by assuming that the hydrostatic head of the reservoir at the cessation of subsidence is controlled by the vent elevation. Using a magma density of  $2.8 \times 10^3 \text{ kg/m}^3$ , Decker and others calculate a pressure change of 0.085 MPa per mrad of summit tilt. If the magma-reservoir roof behaves to some degree like a piston, the change in reservoir pressure could be less than 0.085 MPa/mrad.

## MAGMA DENSITY

The vertical pressure gradient,  $\nabla P_m$ , at a given depth,  $y$ , within a static column of magma is given by

$$\nabla P_m(y) = \rho_m(y) \cdot g, \quad (9)$$

where  $\rho_m(y)$  is the magma density at a given depth, and  $g$  is the acceleration of gravity,  $9.8 \text{ m/s}^2$ . A typical magma density of  $2.6 \times 10^3 \text{ kg/m}^3$  produces a pressure gradient of about 26 MPa/km or 260 bars/km (fig. 53.7A). If the driving pressure simply equals the magma pressure (that is, if  $S(y) = 0$ ), then the stress-intensity factors at the top ( $K^{+a}$ ) and bottom ( $K^{-a}$ ) of the dike are given by

$$K^{+a} = P_o \sqrt{a} - \frac{1}{2} \nabla P_m a^{3/2}, \quad (10a)$$

$$K^{-a} = P_o \sqrt{a} + \frac{1}{2} \nabla P_m a^{3/2}, \quad (10b)$$

where  $P_o$  is the excess magma pressure at the dike center. The first

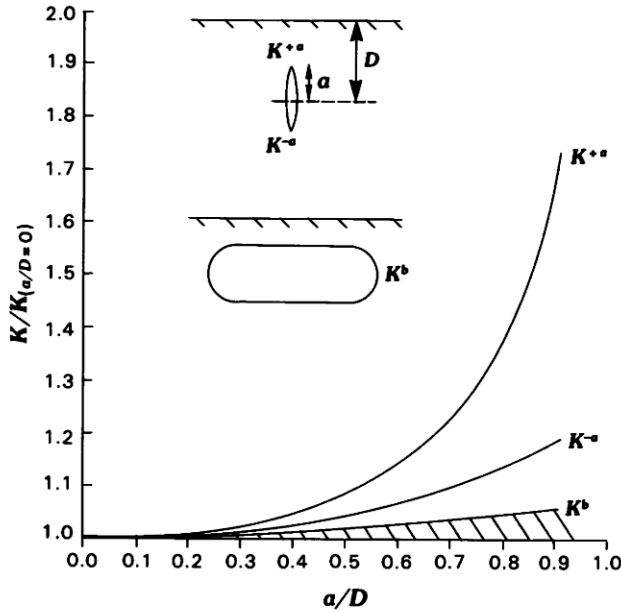


FIGURE 53.5.—Effect of proximity of the Earth's surface on the stress-intensity factors at the top ( $K^{+a}$ ), bottom ( $K^{-a}$ ), and downrift edge ( $K^b$ ) of a dike subjected to a uniform driving pressure. Values of  $K$  are normalized to those for a crack in an infinite body.  $K^{+a}$  and  $K^{-a}$  are calculated for a two-dimensional dike using the method of Pollard and Holzhausen (1979); the range of values for  $K^b$  (shaded) was calculated by Shah and Kobayashi (1973) for elliptical cracks with varying ratios of  $a/b$ . Insets show idealized dike geometry (see fig. 53.3).

term in these equations gives the value of  $K$  due to a uniform driving pressure  $P_o$  (eq 4), and the second term gives the value of  $K$  due to a driving pressure that varies linearly from a value of  $-\nabla P_m a$  at  $y = +a$  to  $\nabla P_m a$  at  $y = -a$  (Secor and Pollard, 1975). For a given  $P_o$ , a decrease in magma density increases  $K^{+a}$  and decreases  $K^{-a}$ , thus promoting upward migration of the dike. If  $P_o$  remains unchanged, a change in magma density does not alter  $K^b$ , because the effect of a change in magma pressure at a height  $y$  above the dike center is balanced by an equal and opposite change at  $-y$ .

VESICULATION

Vesiculation reduces magma density and thus reduces the magma pressure gradient within a dike. In a dike in which uniformly vesiculated magma rests on unvesiculated magma, the magma pressure above the boundary is increased, relative to a dike in which vesiculation is absent (figure 53.7B). The effect of this increase on dike propagation can be assessed through the use of superposition. The driving pressure in a dike with vesiculated magma above a height  $y'$  is equal to that in the absence of vesiculation plus that produced by a pressure which increases linearly from a value of zero at  $y'$  (fig. 53.8). The gradient of this driving pressure,  $\nabla P_v$ , is the difference between the pressure gradients within the vesiculated and unvesiculated magma.

The effect of vesiculation on the stress-intensity factor at the dike top, denoted as  $K_v^{+a}$ , can be evaluated by integrating the effects of point loads (Broek, 1982, p. 78) that give the driving-pressure distribution  $\Delta P = \nabla P_v [y - y']$ , where  $y > y'$  (fig. 53.8). The result is

$$K_v^{+a} = f(y'/a) \nabla P_v a^{3/2}, \tag{11}$$

where  $f(y'/a)$  is a function of  $y'/a$  that is illustrated in figure 53.9A for  $y'/a > 0$ ; that is, for vesiculation originating at or above the dike center.

The effect of the free surface on  $K_v^{+a}$  as a function of  $y'/a$ , for  $a/D = 0.86$ , is shown in figure 53.9B. As  $y'/a$  increases, the effect of the free surface diminishes, and for vesiculation occurring near the dike top it can be neglected.

The relations of the stress-intensity factors at the dike bottom,  $K_v^{-a}$ , and downrift edge,  $K_v^b$ , due to vesiculation plotted against height of vesiculation,  $y'/a$ , are shown in figure 53.9C. Both stress intensities are normalized by  $K_v^{+a}$ . When vesiculated magma is present only near the dike top,  $K_v^{+a}$  is much greater than either  $K_v^{-a}$  or  $K_v^b$ , and the effect of vesiculation on stress intensities at the dike bottom or downrift edge may be neglected. Thus vesiculation

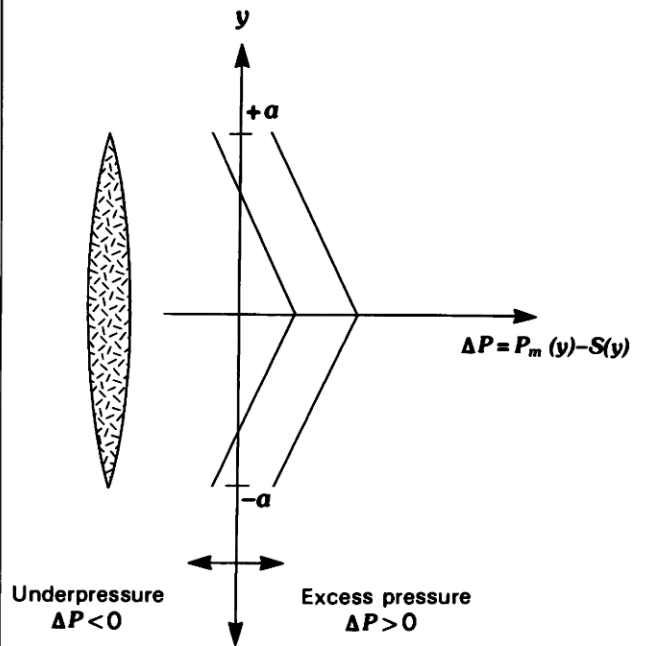


FIGURE 53.6.—Schematic diagram of two possible driving-pressure distributions that would promote the growth of blade-like dikes. If the driving pressure at the dike center is sufficiently greater than at the dike top or bottom, then  $K^b > K^a$ . For the right-hand curve, there is an excess pressure along the entire dike height. For the left-hand curve, the excess pressure at the dike center is sufficient to keep the dike open for its entire height, even though an underpressure acts locally at the dike top and bottom.  $P_m(y)$ , magma pressure;  $S(y)$ , remote stress;  $\Delta P$ , net driving pressure;  $a$ , dike half-height.

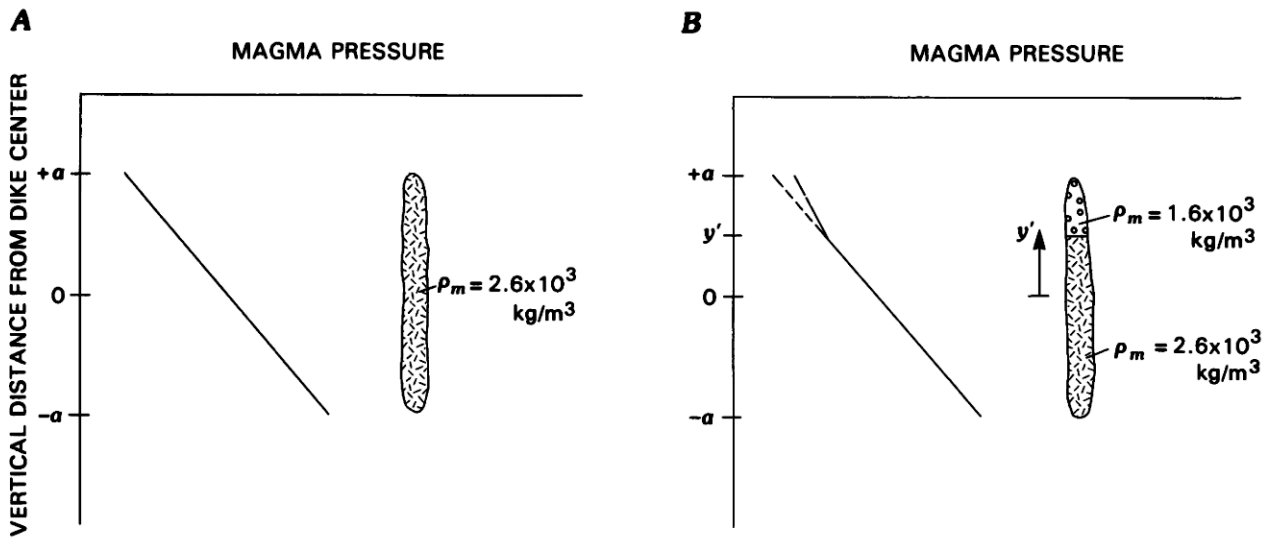


FIGURE 53.7.—Schematic diagram of vertical pressure variation in dikes. **A**, Pressure in a dike consisting of a static column of magma of density  $2.6 \times 10^3 \text{ kg/m}^3$ . **B**, Pressure in a dike consisting of a static column of magma with a density of  $2.6 \times 10^3 \text{ kg/m}^3$  overlain above a height  $y'$  by vesiculated magma with a density of  $1.6 \times 10^3 \text{ kg/m}^3$ .

promotes upward growth of the dike, while affecting downward and lateral growth relatively little. Dike thickness is similarly affected relatively little by pressure applied only near the dike top.

VISCIOUS PRESSURE LOSS

The pressure gradients within a dike during flow will deviate from those within a static body of magma. We approximate these

pressure gradients by assuming laminar flow of a viscous fluid through a channel of uniform thickness. Following Bird and others (1960, p. 59) we have

$$\nabla P_{mi} = -2 \frac{V_i \eta}{(t/2)^2}, \tag{12}$$

where  $\nabla P_{mi}$  is the magma-pressure gradient minus the gravitational-pressure gradient in the  $x_i$  direction,  $V_i$  is the velocity of the magma

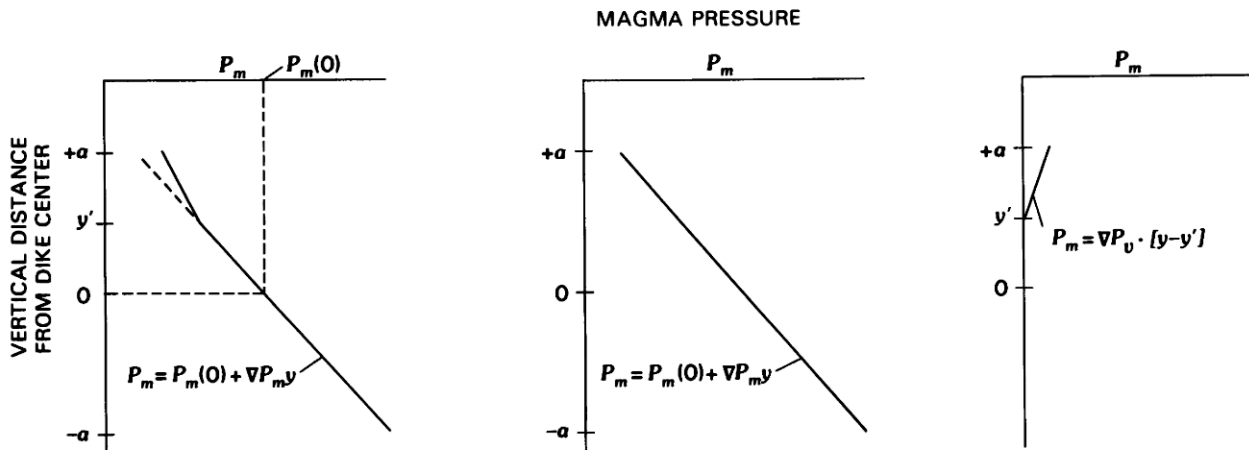


FIGURE 53.8.—The pressure within a dike containing vesiculated magma near its top (graph at left) can be expressed as a sum of the magma pressure in the absence of vesiculation (center) plus a pressure that increases linearly from the point at which vesiculation occurs (right). That pressure gradient,  $\nabla P_v$ , is equal to the difference in pressure gradients between the vesiculated and unvesiculated magmas.

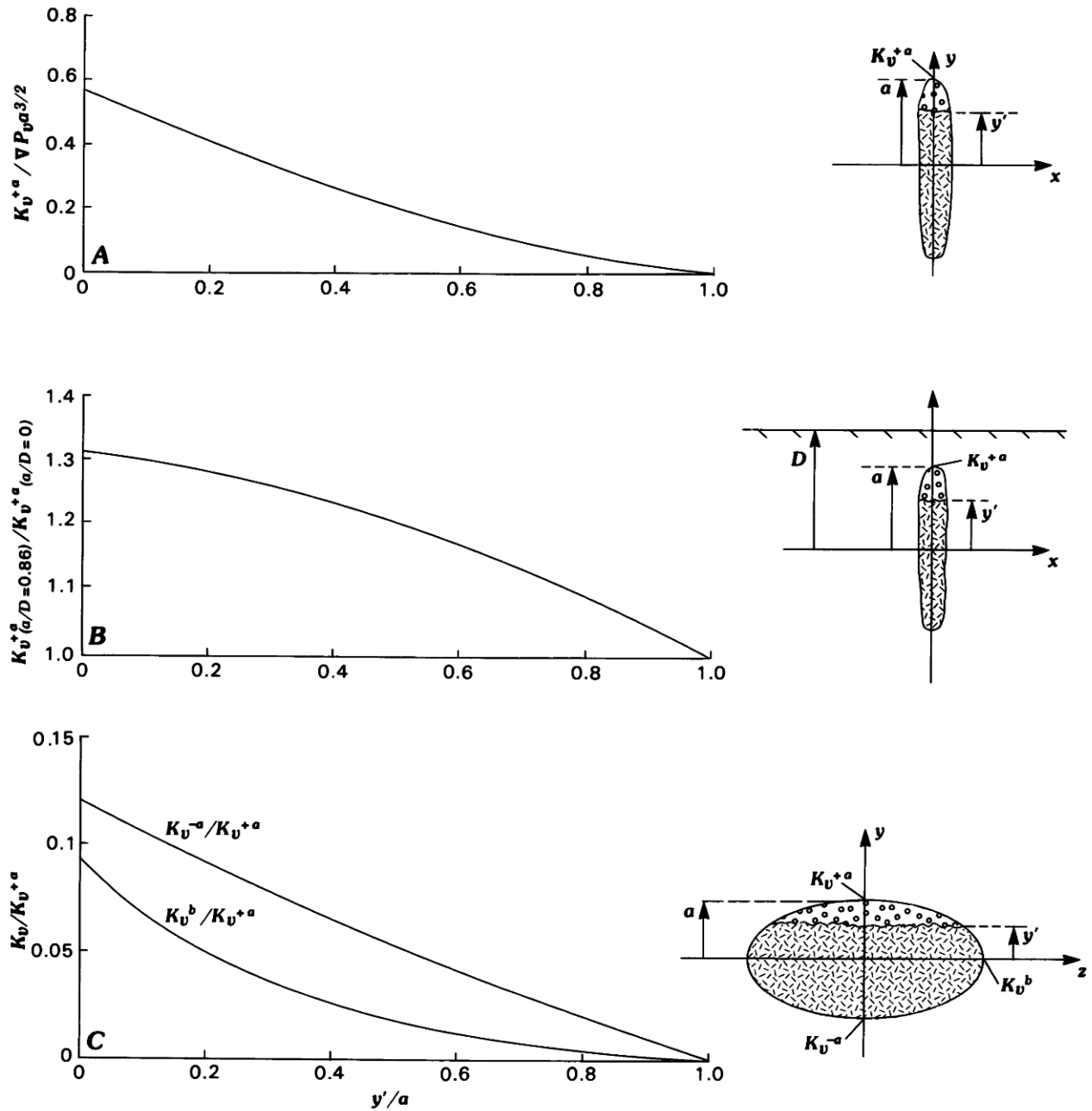


FIGURE 53.9.—Graphs showing effects of vesiculated magma in upper part of a dike.  $y'$ , height above dike center of base of vesiculated magma;  $a$ , dike half-height;  $D$ , depth to dike center. **A**, Graph of the coefficient  $f(y'/a)$  for obtaining the stress-intensity factor at the dike top ( $K\pi\pi_v^{+a}$ , eq. 11). Note that  $K_v^{+a}$  decreases as the extent of vesiculation decreases. **B**, Effect of the Earth's surface on the stress-intensity factor due to vesiculation at the dike top as a function of  $y'/a$  for  $a/D = 0.86$ . Note that the effect of the free surface diminishes as the size of the vesiculated region decreases, and that for  $y'/a > 0.8$  the free surface causes only a 10 percent or less increase in  $K_v^{+a}$ . **C**, Stress-intensity factors due to vesiculation at the dike bottom ( $K_v^{-a}$ ) and downrift edge ( $K_v^b$ ) as a function of  $y'/a$ . Note that the values of  $K$  normalized with respect to the stress intensity at the dike top are very small for most values of  $y'/a$ , so this effect may be neglected.

in the  $x_i$  direction in the center of the channel,  $\eta$  is the magma viscosity, and  $t$  is the channel thickness.

Delaney and Pollard (1981) estimated the upward flow velocity of magma during the initiation of the 1959 Kilauea Iki fissure eruption to be 0.1 m/s. Using a typical magma viscosity of 100 Pa · s and a dike thickness of 1 m, they calculated the driving-pressure gradient for upward magma flow to be 0.05 MPa/km. This is only about 0.2 percent of the pressure gradient due to the weight of a static column of magma with a density of  $2.6 \times 10^3$  kg/m<sup>3</sup> and about 1 percent of the difference in pressure gradients between a static column of magma and a column of rock with a density of  $2.3 \times 10^3$  kg/m<sup>3</sup>. Vertical flow rates, and therefore vertical pressure gradients due to flow, are likely to be even less for subsurface dikes. Thus we neglect vertical magma flow and relate the vertical magma-pressure gradient only to the magma density, as in figure 53.7.

Although lateral magma-pressure gradients do not enter our model explicitly, they are likely to be important in determining the site of rift-zone fissure eruptions. To estimate these gradients, we take as typical of Kilauea dikes a lateral velocity of 0.5 m/s and a thickness of 1 m (Delaney and Pollard, 1981). From equation 12, this requires a magma-pressure drop of 0.2 MPa/km. By comparison, the slopes of both the east and southwest rift zones of Kilauea are about 25 m/km. If a dike with magma of density  $2.6 \times 10^3$  kg/m<sup>3</sup> travels at a constant depth within these rift zones, the decrease in elevation would lead to a magma-pressure increase at a fixed depth of about 0.65 MPa/km.

#### REMOTE-STRESS DISTRIBUTION SOURCES OF THE REMOTE STRESS

Given the nature of the vertical pressure distribution within dikes illustrated in figure 53.7, the source of the nonlinear driving pressure distributions required for the growth of blade-like dikes (fig. 53.6) must arise from variations in the remote stress  $S(y)$  acting perpendicular to the dike plane. Several possible mechanisms that could generate the required stress-versus-depth curves at Kilauea are discussed in this section.

#### CRUSTAL DENSITY

Combined seismic and gravity modeling of Kilauea and Mauna Loa indicates that the density within the upper two kilometers of these volcanoes is considerably less than that of unvesiculated magma, and that the density below is considerably greater. The density structure along a section through the Kilauea and Mauna Loa summit regions (Zucca and others, 1982) is shown in figure 53.10. The surface density of  $2.3 \times 10^3$  kg/m<sup>3</sup> corresponds to an average density for vesiculated lava flows (Kinoshita and others, 1963). The density of  $2.9 \times 10^3$  kg/m<sup>3</sup> at depth might represent submarine lavas (Moore and Fiske, 1969; Swanson and others, 1976), solidified intrusions (Hill and Zucca, chapter 37), or flows with vesicles now filled with hydrothermal minerals. If the state of stress in the rift zone were lithostatic and the remote horizontal stress were equal to the pressure induced by the overlying column of rock,

then  $S(y)$  would be of the form depicted in figure 53.6 (fig. 53.11A). Assuming a magma density of  $2.6 \times 10^3$  kg/m<sup>3</sup>, the local density contrasts between the magma and the wall rock result in a driving pressure that decreases toward the dike top and bottom at a rate of 3 MPa/km. Interpretation of the density structure of the Icelandic crust (Palmason, 1971) is also consistent with the hypothesis that local density contrast is a sufficient mechanism for the generation of blade-like dikes.

#### GRAVITATIONAL LOADING OF THE VOLCANIC RIDGE

It is commonly assumed that dikes are intruded perpendicular to the local least compressive stress (Anderson, 1938). The numerous parallel dikes and the relative scarcity of sills in eroded Hawaiian rift zones suggests that the stress perpendicular to the rift zone is consistently less compressive than both the vertical stress and the rift-parallel horizontal stress. This implies that some horizontal tensile stress is superimposed on a hydrostatic state of stress. Fiske and Jackson (1972) suggested that the source of this tensile stress is gravity loading of the volcanic edifice. They injected fluid into ridge-shaped gelatin models and produced "dikes" that propagated along the strike of the ridge with a nearly fixed height and depth, raising the possibility that this superimposed stress was not only responsible for dike orientation, but was also of the form necessary to limit their upward and downward growth.

Analyses of the gravitational stresses acting perpendicular to the axial plane of a ridge using numerical methods (McTigue and Mei, 1981) and finite-element models (James Dieterich, written commun., 1985) indicate that the stress is compressive at the surface and decreases or increases only slowly with depth. This generates a stress curve of the form that could prevent the dike top from rising (fig. 53.11B). However, the finite-element analysis indicates that the gelatin models were effective in containing the bottom of the propagating dike because of the great vertical exaggeration of the ridge shape and the high Poisson's ratio of gelatin (about 0.49). When realistic slopes and a Poisson's ratio appropriate for rock (about 0.25) are used, the resulting remote stress increases less rapidly than the magma pressure with depth, and barring an increase in  $K_c$  with depth, dikes intruded into the rift zone would continue propagating downward and not be trapped within the upper part of the crust (fig. 53.11B).

#### PREVIOUSLY INTRUDED DIKES

Following magma solidification, the stresses generated in the rift zone by a dike remain. The compressive stress within the rift zone is increased to values close to the magma pressure near the dike center and decreased near the dike top and bottom (Pollard and Segall, in press). This stress distribution would encourage successive dikes to be emplaced above or below the previous one, or else far to the side (fig. 53.11C). Possible examples of dikes that intruded at greater depths than previous dikes include the February 1980 intrusion at Krafla (Bryndis Brandsdottir, oral commun., 1985) and the June 1982 southwest-rift-zone intrusion at Kilauea (fig. 53.1). After several intrusions,  $S(y)$  would approach  $P_m(y)$

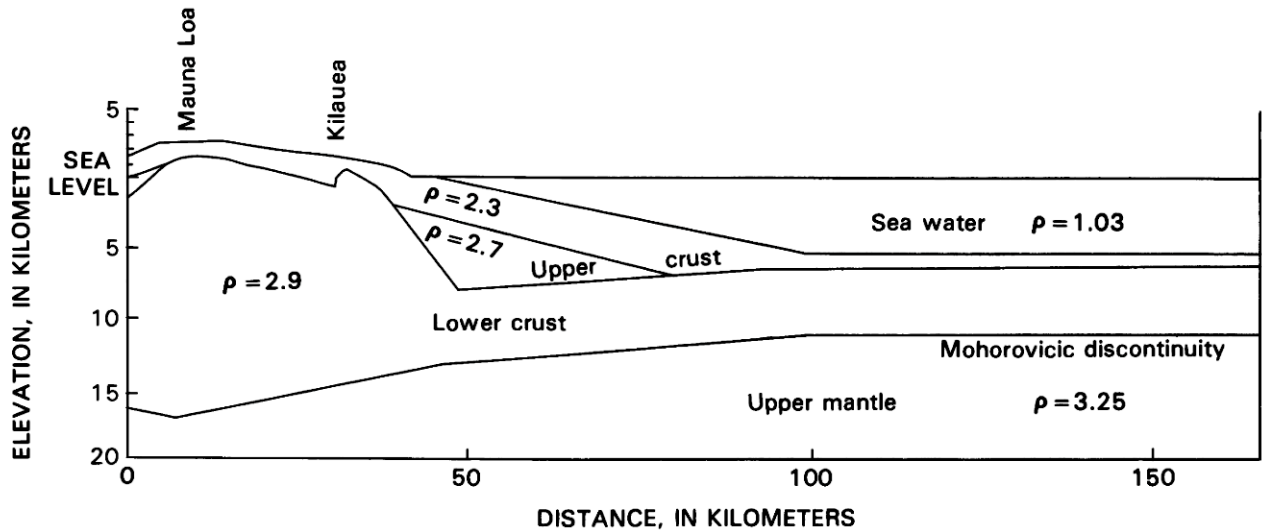


FIGURE 53.10.—Distribution of density ( $\rho$ , in  $10^3 \text{ kg/m}^3$ ) in a model section through Kilauea and Mauna Loa Volcanoes (after Zucca and others, 1982). The modeled increase in density from  $2.3 \times 10^3 \text{ kg/m}^3$  to  $2.9 \times 10^3 \text{ kg/m}^3$  at about 2 km beneath the surface provides a mechanism for confining both magma reservoirs and dikes to shallow depths.

throughout the rift zone, and intrusions would cease unless  $P_m(y)$  increased.

#### FAULTING

In order for successive dikes to be intruded into the rift zone without the magma pressure increasing monotonically through time, the rift zone must somehow behave inelastically and allow the stresses induced by dike intrusion to relax. One possible mechanism for this relaxation is slip along major faults at depth (Swanson and others, 1976). In 1975 a magnitude-7.2 earthquake occurred near Kalapana on the southeast coast of the Island of Hawaii. This earthquake seemed to have a direct effect on the intrusion-to-extrusion ratio of dikes emanating from the Kilauea magma reservoir (Klein, 1982).

James Dieterich (written commun., 1985) has modeled the stress induced by slip along a segment of a fault whose location and orientation are within the ranges inferred for the Kalapana fault. His results indicate that such motion superimposes tension within the rift zone that reaches a maximum about 3 km below the surface. This yields a driving-pressure distribution of the proper form for stabilizing a dike top and bottom (fig. 53.11D). The magnitude of this tension appears to be sufficient for the intrusion of only one or two overlapping dikes of average width before another major earthquake is required. The absence of frequent magnitude-7.2 earthquakes suggests that additional stress-relaxation processes may be active in the rift zone.

#### ANALYSIS FOR THE REMOTE STRESS

From the principle of superposition, the driving-pressure distribution  $\Delta P(y)$  depicted in figure 53.6 can be represented as the

sum of a uniform driving pressure  $P_o$  (equal to the excess magma pressure at the dike center) and two linearly varying driving-pressure distributions, each acting over one-half of the dike, which tend to pull the dike walls inward (fig. 53.12). The linear driving-pressure distributions are given by  $\Delta P(y) = -\nabla P_u |y|$ ,  $y > 0$ , and  $\Delta P(y) = -\nabla P_l |y|$ ,  $y < 0$ , where  $\nabla P_u$  and  $\nabla P_l$  are the gradients in the driving pressure acting on the upper and lower halves of the dike, respectively. The stress intensities produced at the top ( $K^{+a}$ ) and bottom ( $K^{-a}$ ) of a two-dimensional dike by these driving pressure distributions can be evaluated by superposing the solutions for cracks subjected to symmetric (Pollard, 1976) and anti-symmetric (Secor and Pollard, 1975) loads. The results are

$$K^{+a} = -\left(\frac{1}{\pi} + \frac{1}{4}\right) \nabla P_u a^{3/2}, \quad (13a)$$

$$K^{-a} = -\left(\frac{1}{\pi} - \frac{1}{4}\right) \nabla P_u a^{3/2}, \quad (13b)$$

for the pressure acting on the upper half of the dike, and

$$K^{+a} = -\left(\frac{1}{\pi} - \frac{1}{4}\right) \nabla P_l a^{3/2}, \quad (13c)$$

$$K^{-a} = -\left(\frac{1}{\pi} + \frac{1}{4}\right) \nabla P_l a^{3/2}, \quad (13d)$$

for the pressure acting on the lower half of the dike. When these equations are combined with equation 4 for a uniform driving pressure  $P_o$ , the stress-intensity factors for the driving-pressure distribution depicted in figure 53.12B are given by

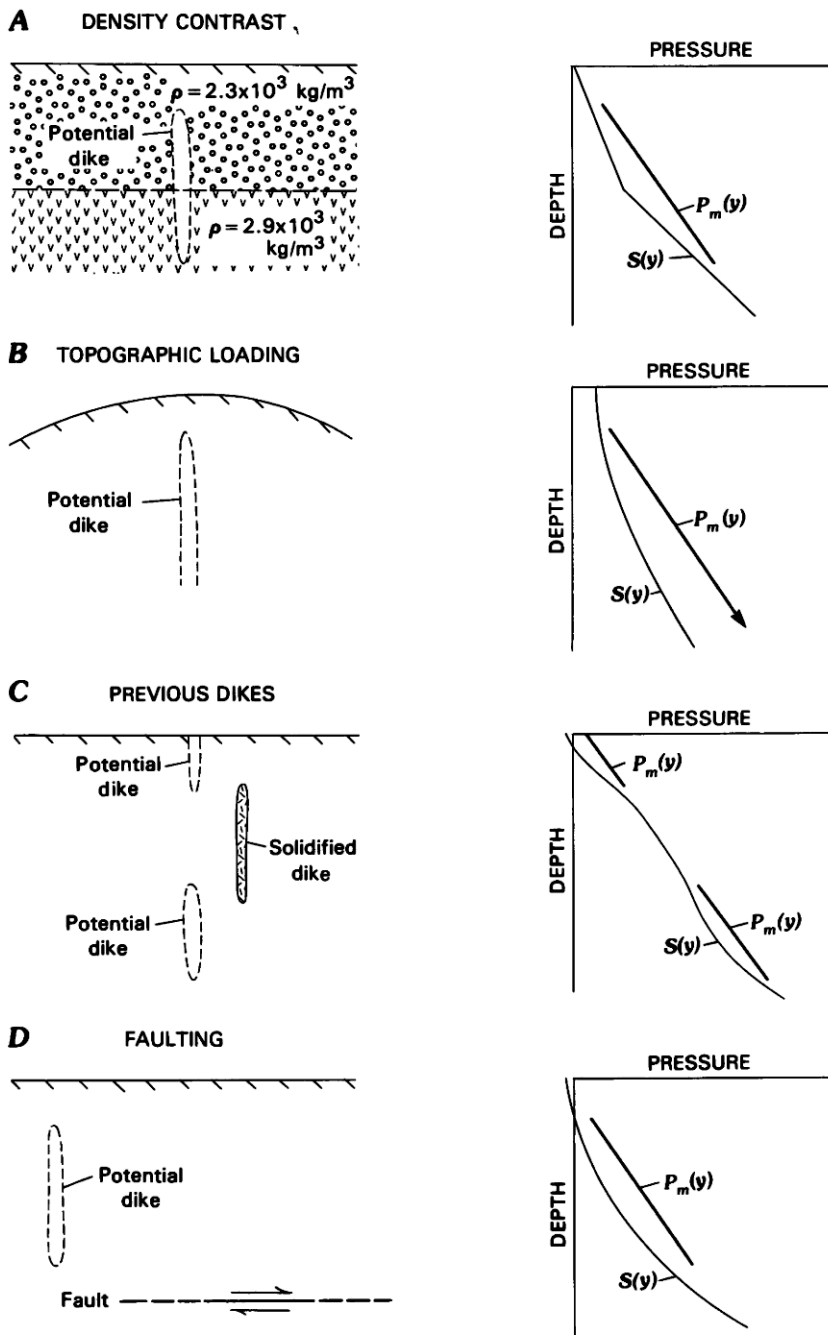


FIGURE 53.11.—Diagrams showing various mechanisms (left) and the resulting remote stress curves (right) possibly acting within a rift zone. Depths of potential dike intrusions shown.  $S(y)$ , remote stress;  $P_m(y)$ , magma pressure. **A**, Lithostatic state of stress in a density-stratified rift zone of the type modeled by Zucca and others (1982). **B**, Stresses due to topographic loading of the volcanic ridge, from James Dieterich (written commun., 1985). Compressive stress near the surface can prevent the dike top from propagating up, but compressive stress does not increase rapidly enough with depth to prevent the bottom from continuing to propagate down. **C**, Stresses induced by previous intrusion of dikes. Subsequent dikes would tend to be intruded above, below, or well to the side of earlier ones. **D**, Stresses generated by motion along a Kalapana-like fault, from James Dieterich (written commun., 1985). The depth of the maximum superimposed tension depends upon the fault dip and the location of slip.

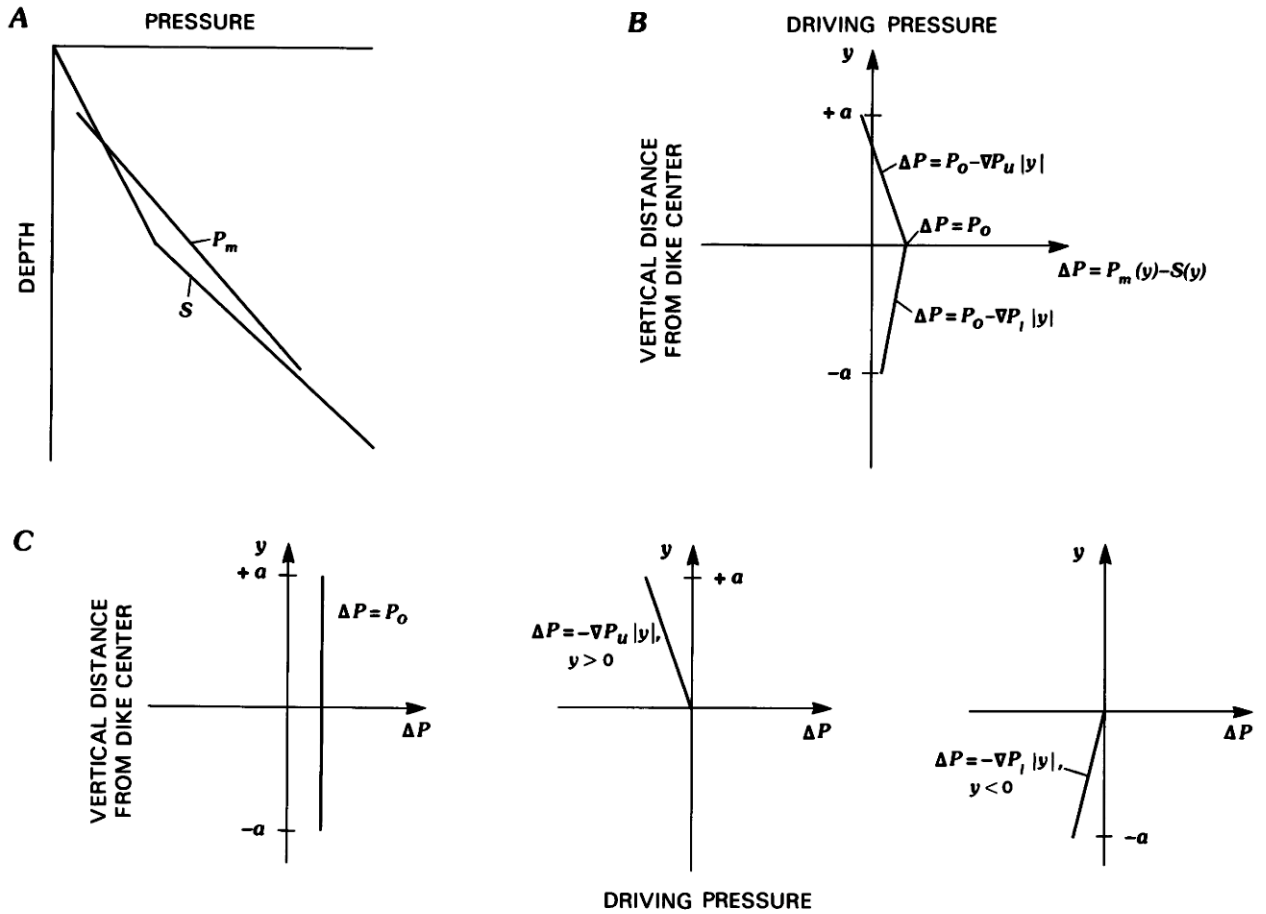


FIGURE 53.12.—Diagrams of stress distributions with depth. **A**, Remote stress  $S$  from idealized density structure (fig. 53.11A) and magma pressure  $P_m$  caused by static weight of magma (fig. 53.7A). **B**, Distribution of driving pressure  $\Delta P(y)$  resulting from  $P_m - S$  as depicted in **A**. **C**, Driving pressure in **B** represented as the sum of a uniform driving pressure (left) equal to the excess pressure acting at the dike center ( $P_o$ ), and two linearly varying driving-pressure distributions ( $-\nabla P_u|y|$  and  $-\nabla P_l|y|$ ), acting over the upper and lower halves of the dike (center and right).

$$K^{+a} = P_o \sqrt{a} - \left(\frac{1}{\pi} + \frac{1}{4}\right) \nabla P_u a^{3/2} - \left(\frac{1}{\pi} - \frac{1}{4}\right) \nabla P_l a^{3/2}, \tag{14a}$$

$$K^{-a} = P_o \sqrt{a} - \left(\frac{1}{\pi} - \frac{1}{4}\right) \nabla P_u a^{3/2} - \left(\frac{1}{\pi} + \frac{1}{4}\right) \nabla P_l a^{3/2}. \tag{14b}$$

In a similar fashion, the average dike thickness is found to be

$$\bar{t} = \frac{1-\nu}{\mu} \left( \frac{\pi}{2} P_o a - 0.33 \nabla P_u a^2 - 0.33 \nabla P_l a^2 \right). \tag{15}$$

To estimate  $K^b$  at the downrift edge of the dike resulting from a driving-pressure distribution,  $\Delta P = -\nabla P|y|$ , acting on the upper or lower half of the dike, we calculate  $K^b$  for a disc-shaped crack of radius  $a$  by integrating the contributions from applied point loads (Tada and others, 1973) giving the distribution  $\Delta P = -\nabla P|y|$ ,  $0 < y < a$ . The result is

$$K^b = -0.053 \nabla P a^{3/2}. \tag{16}$$

The low coefficient illustrates the rather small effect such gradients have on the stress intensity at the downrift edge of the dike. Combining this with (7) for the contribution to  $K^b$  from the uniform applied load, we derive

$$K^b = \frac{2}{\pi} P_o \sqrt{a} - 0.053 \nabla P_u a^{3/2} - 0.053 \nabla P_l a^{3/2} \tag{17}$$

for the driving pressure depicted in figure 53.12B.

The effect of the Earth's surface on each of the superposed boundary conditions in figure 53.12 is presented as a function of  $a/D$  in figure 53.13A. This graph can be thought of as providing correction factors to equation 14 to be used when superposing solutions for particular values of  $a/D$ . For a given  $a/D$ , the contribution to  $K^{+a}$  or  $K^{-a}$  from a particular term in equation 14

should be multiplied by the ordinate of the curve in figure 53.13 corresponding to that term. Because  $K^b$  is not very sensitive to  $a/D$  (fig. 53.4), its value in an infinite body will be used. An equivalent graph for average dike thickness is presented in figure 53.13B.

#### SUMMARY OF THE FACTORS AFFECTING DIKE PROPAGATION

We have discussed various parameters that are important to the dike propagation process and, through the calculation of the stress-intensity factors  $K^a$  and  $K^b$ , have analyzed their effects on lateral and vertical propagation. A blade-like dike shape and the presence of the Earth's surface both enhance upward propagation and eruption relative to lateral propagation. Observation of continued subsurface lateral propagation requires the dike driving pressure to be such that it overcomes these geometric effects. A driving pressure that is greater at the dike center than at the dike top and bottom could satisfy this condition. Since the pressure gradient within a column of unvesiculated magma is uniform, and since vesiculation increases the driving pressure only at the dike top, the origin of this driving pressure must be the remote stress. Processes that could contribute to the required remote-stress distribution at Kilauea include density stratification of the rift zone, gravitational loading, previously intruded dikes, and slip along faults.

Equations 14a, 14b, 17, and 15 were developed to calculate the stress-intensity factors at the dike top, bottom, and downrift edge, and the average dike thickness, for a driving pressure that is greatest at the dike center and decreases linearly toward the top and bottom. These equations can be corrected for the effect of the free surface using the graph in figure 53.13. The stress-intensity factor at the dike top (eq 14a) can be modified to include the effects of vesiculation (eq 11), but the effect of the free surface on equation 11, and the effect of vesiculation on equations 14b, 15, and 17 can be neglected. In the following section we show how these equations may be applied to analyze a rift-zone intrusion.

#### APPLICATION TO THE INTRUSIVE EVENT OF AUGUST 1981

The above analysis makes it possible to estimate the magma pressure and the horizontal remote-stress distribution acting perpendicular to the rift axis for particular dikes whose geometry is known. We begin by assuming that the magma is unvesiculated, so that the magma pressure variation with depth is given by a line segment of constant slope. We also assume that the remote stress can be adequately represented by two linearly varying line segments (fig. 53.12), each of which acts on one-half of the dike. In general, a dike center is not constrained to be positioned at a kink in the stress distribution. Nevertheless, useful insight into the nature of the driving pressure distribution is obtained by employing this assumption. We assume that  $K_c$  is independent of depth, so that  $K^{+a} = K^{-a} = K_c$  at the moment the dike ceases to propagate in the vertical direction. Finally, we assume that the shape of the dike determined using geodetic data collected after the cessation of

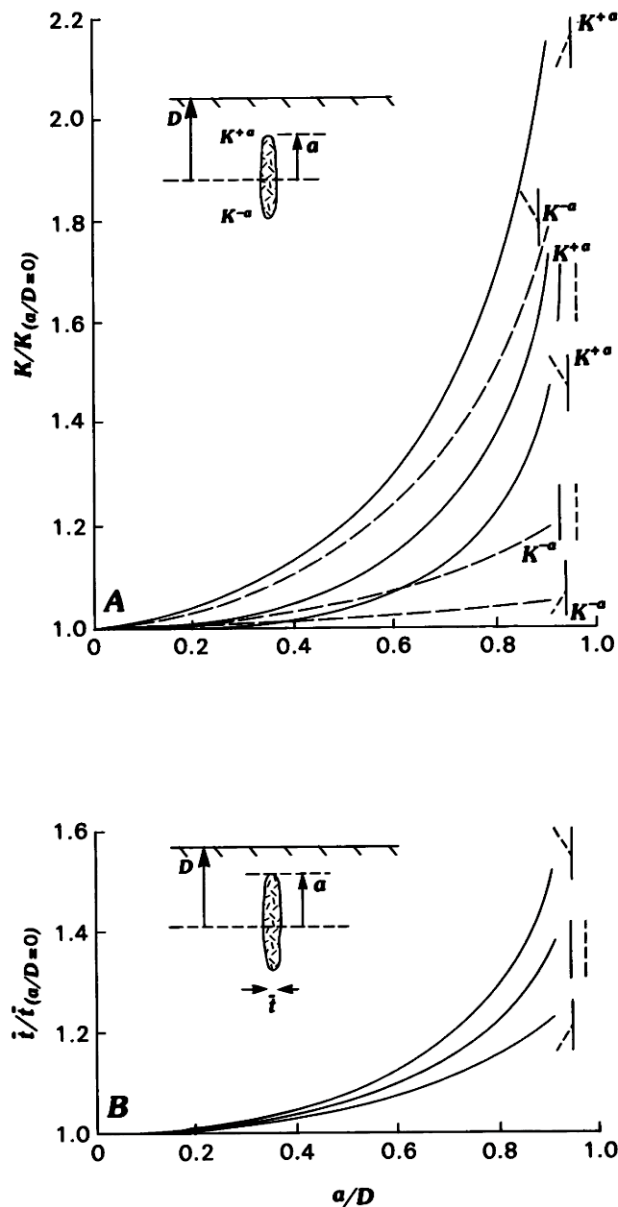


FIGURE 53.13.—Diagrams showing effect of proximity of the Earth's surface on stress-intensity factors and average dike thickness. *A*, Effect of the Earth's surface on stress-intensity factors at the dike top (solid lines) and bottom (dashed lines) as a function of  $a/D$  for components of the driving pressure in fig. 53.12C, identified by the schematic diagrams to the right. *B*, Effect of the Earth's surface on average dike thickness as a function of  $a/D$  for components of the driving pressure in fig. 53.12C.

intrusive activity is approximately the shape of the dike when it attained its maximum height.

In August 1981 a dike approximately 25 km long was intruded into the southwest rift zone of Kilauea (fig. 53.1). From geodetic

data, Pollard and others (1983) estimated a dike half-height of 1.5 km, a depth of 1.75 km, an average thickness of 1.4 meters, and a dip of 82°. Although difficulty was encountered in reproducing the displacement data for the southeast half of the profile using the elastic model, we use these geometric parameters for our analysis. Abundant ground cracks that formed above the dike are good evidence for a shallow dike top; in combination with the large ratio of  $a/D$ , they indicate that interaction of the dike with the free surface should be included. We ignore the dip of the dike, which alters neither the gradients in driving pressure nor the free-surface correction by more than 1–2 percent.

Using figure 53.13 and a value for  $a/D$  of 0.86 to obtain the free-surface correction factors for equations 14 and 15, we have

$$K^{+a} = 1.52P_o\sqrt{a} - 1.31\left(\frac{1}{\pi} + \frac{1}{4}\right)\nabla P_u a^{3/2} - 1.86\left(\frac{1}{\pi} - \frac{1}{4}\right)\nabla P_l a^{3/2}, \quad (18a)$$

$$K^{-a} = 1.17P_o\sqrt{a} - 1.63\left(\frac{1}{\pi} - \frac{1}{4}\right)\nabla P_u a^{3/2} - 1.05\left(\frac{1}{\pi} + \frac{1}{4}\right)\nabla P_l a^{3/2}, \quad (18b)$$

$$\bar{t} = \frac{1-\nu}{\mu} \left( 1.29\frac{\pi}{2}P_o a - 1.39(0.33)\nabla P_u a^2 - 1.19(0.33)\nabla P_l a^2 \right). \quad (19)$$

Setting  $K^{+a} = K^{-a}$ , we find

$$\nabla P_l a = 1.34\nabla P_u a - 0.74P_o, \quad (20)$$

which we then substitute for  $\nabla P_l a$  in equations 17 through 19. To restrict the range of values of  $P_o$  and  $\nabla P_u$ , we first use the requirement that  $K^a > 0$ . From equation 18a we find

$$P_o > 0.57\nabla P_u a. \quad (21)$$

Next we use the requirement that  $K^a < K^b$  for a dike with a stable height but a propagating downrift edge; using equations 17 and 18a, we find

$$P_o < 0.84\nabla P_u a. \quad (22)$$

Limiting remote stress and magma pressure curves for a dike with a half-height of 1,500 m and a depth of 1,750 m are shown in figures 53.14A and 53.14B. The magma has a density of  $2.6 \times 10^3 \text{ kg/m}^3$  and thus an internal pressure gradient of 26 MPa/km. We specify that the remote stress has a value of zero at the surface. The gradient of the driving pressure acting on the upper half of the dike in figure 53.14A is 3 MPa/km, or approximately that generated by the local density contrast between the magma and the wall rock. Modeling by James Dieterich (written commun., 1985) indicates that both gravity loading and slip on a master fault at depth superimpose tensile stresses that increase with depth in the upper few kilometers of the volcano, so 3 MPa/km is likely to be a

lower limit for this gradient. The gradient of the driving pressure acting on the upper half of the dike in figure 53.14B is 11 MPa/km. We show below that this is an upper limit if the hydrostatic head of the magma is higher than 350 m below the surface. The remote stress acting on the lower half of the dike in figure 53.14 is the average of the relatively narrow range of  $\nabla P_l$  obtained from equation 20 and the constraint that  $P_o$  be in the range  $0.57\text{--}0.84 \nabla P_u a$ .

The left-hand magma-pressure curve in figure 53.14A corresponds to  $P_o = 0.57 \nabla P_u a$  (eq 21), and the right-hand curve to  $P_o = 0.84 \nabla P_u a$  (eq 22). A  $P_o$  less than the former would produce a  $K^a$  less than zero, in which case the dike could not have propagated to its required height, and a  $P_o$  greater than the latter would violate the requirement that  $K^a < K^b$ . Allowable magma-pressure curves for this value of  $\nabla P_u$  therefore lie between the limits indicated. The horizontally exaggerated cross-sectional forms resulting from these two driving-pressure distributions are shown in the upper right of figure 53.14A. In figure 53.14B, the lower magma-pressure curve has a hydrostatic head beneath the dike top, and so equations 17–19 do not apply. To treat this case, we assume that unvesiculated magma rises to its hydrostatic head and is capped by a near vacuum. We obtain  $y'$ , calculate  $K^{+a}$  (eq 11), and include this term in the calculation of  $K^{+a}$  (eq 18a). Because of the small effect on  $K^{-a}$ ,  $K^b$ , and  $\bar{t}$ , equations 17, 18b, and 19 need not be modified.

The limiting magma-pressure curves in figures 53.14A and 53.14B require knowledge only of the dike height and depth. In order to restrict the magma-pressure range further, additional constraints are needed. Associated with each magma-pressure curve is a value for  $K^a$  and, given a value for the rock stiffness, an average dike thickness. These are indicated in figure 53.14. Magma-pressure curves generating values of  $K^a$  equal to those for  $K_c$  determined in the laboratory are essentially indistinguishable from those generating a  $K^a$  of zero. Note that the right-hand magma-pressure curve in figure 53.14B is greater than our upper limit of  $100 \text{ MPa} \cdot \text{m}^{1/2}$ . The low values of dike thickness are calculated using laboratory determinations of the shear modulus (30 GPa), and the high values are calculated using estimates of the effective shear modulus from piezomagnetic measurements at Kilauea (3 GPa) (Davis, 1976). Note that the lower values of dike thickness are well below the value of 1.4 m estimated for the 1981 intrusion for each driving-pressure distribution shown.

A summary plot of the driving pressure at the dike center,  $P_o$ , versus the product of the gradient in driving pressure and the dike half-height,  $\nabla P_u a$ , is presented in figure 53.15. The wedge-shaped region (red lines) bounded by  $P_o = 0.57 \nabla P_u a$  (eq 21) and  $P_o = 0.84 \nabla P_u a$  (eq 22) contains all values of  $P_o$  and  $\nabla P_u a$  that are consistent with observed dike-propagation behavior. Points lying below the lower red boundary are unacceptable because the dike could not have propagated to a half-height of 1,500 m, and those lying above the upper red boundary are unacceptable because the dike would have continued propagating vertically and possibly would have erupted. For a given dike height, thickness, and depth, the wedge-shaped region can be contoured for values of the fracture

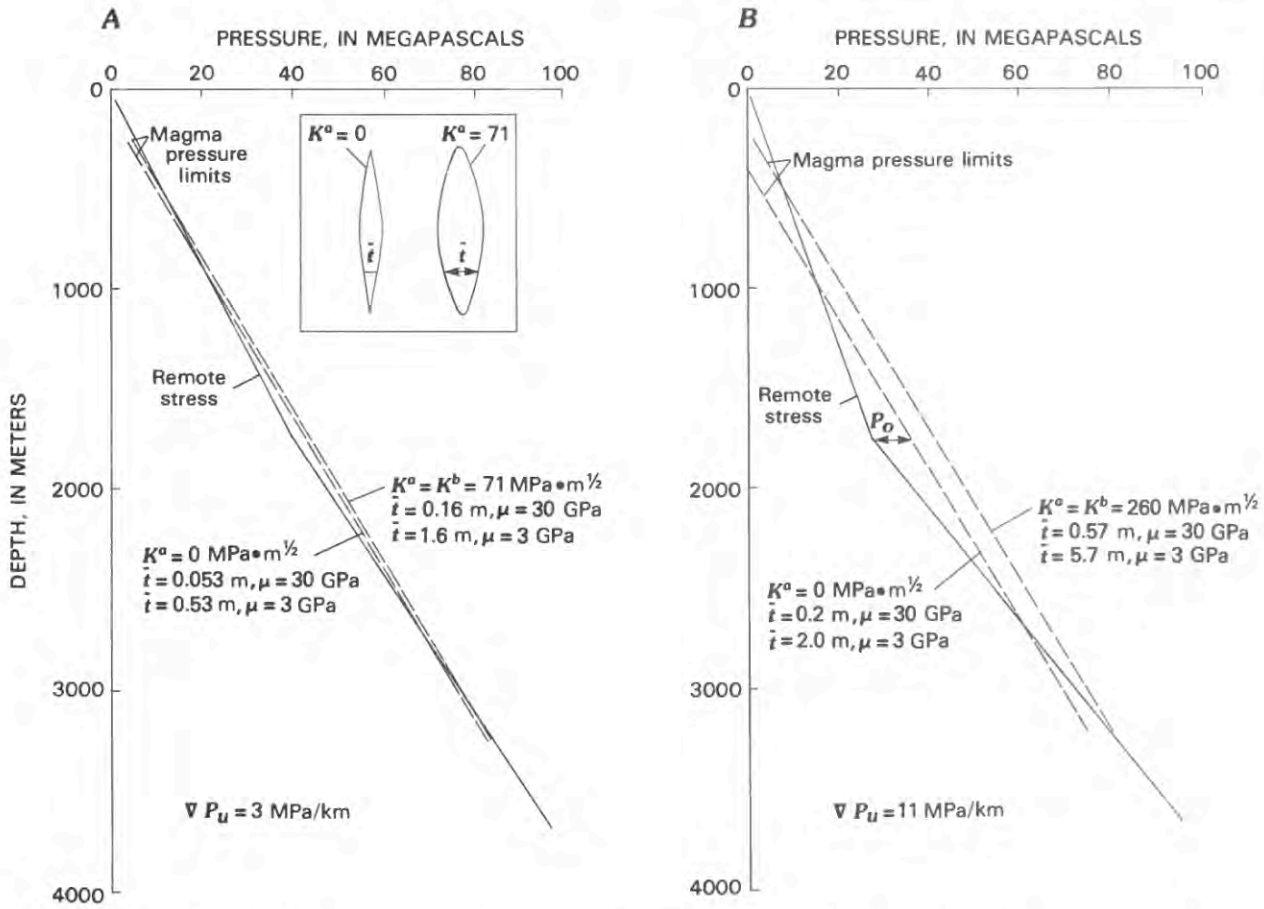


FIGURE 53.14.—Limiting remote-stress and magma-pressure curves for a dike with a height of 1,500 m and a depth of 1,750 m. The magma has a density of  $2.6 \times 10^3 \text{ kg/m}^3$ . The remote stress is constrained to have a value of zero at the surface. The range of allowable values of  $P_o$  is given by the left and right magma pressure curves in each diagram. For any lower  $P_o$ ,  $K^a < 0$ ; for any higher  $P_o$ ,  $K^a > K^b$ . Each magma-pressure curve is associated with a value of  $K^a$ , and, given a value for the shear modulus, an average dike thickness. The average dike thicknesses indicated are for shear moduli of 3 and 30 GPa. The higher shear modulus predicts thicknesses too narrow (<1.4 m). **A**, Curves for  $\nabla P_u = 3 \text{ MPa/km}$ . The inset shows the horizontally exaggerated cross-sectional forms of dikes generated by the limiting magma-pressure curves. **B**, Curves for  $\nabla P_u = 11 \text{ MPa/km}$ .  $K^a$  for the right-hand curve is greater than our upper limit for  $K_c$  of  $100 \text{ MPa} \cdot \text{m}^{1/2}$ .

toughness, rock stiffness, and hydrostatic head of the magma column. These contours will be used to further constrain the driving pressure.

Substituting equation 20 into equation 19 and rearranging yields

$$P_o = 0.42 \nabla P_u a + 0.43 \frac{\bar{t}}{a} \frac{\mu}{(1-\nu)} \quad (23)$$

Thus contours of the dike thickness-to-height ratio times the rock stiffness are straight lines. For  $a = 1,500 \text{ m}$ ,  $\bar{t} = 1.4 \text{ m}$ , and  $\nu = 0.25$ , these lines become contours of the shear modulus,  $\mu$ . Contours for values of  $\mu$  of 1.5 GPa, 3 GPa, and 6 GPa are shown.

Substituting equation 20 into equation 18a and rearranging yields

$$P_o = 0.57 \nabla P_u a + 0.62 \frac{K^{+a}}{\sqrt{a}} \quad (24)$$

Thus contours of  $K^{+a}$  divided by the square root of the dike half-height are also straight lines; on figure 53.15, these contours are parallel to the lower boundary of the wedge-shaped region, for which  $K^a = 0$ . Contours of the lower and upper limits for  $K_c$ , 0 and  $100 \text{ MPa} \cdot \text{m}^{1/2}$ , are shown. If laboratory values ( $K_c \approx 1 \text{ MPa} \cdot \text{m}^{1/2}$ ) represent the upper bound, the stress would be constrained to lie near the lower boundary of the wedge-shaped region.

From figure 53.14, one can derive that the magma pressure in the center of the dike is

$$P_m(0) = D(\rho_m g - \nabla P_u) + P_o, \quad (25)$$

where  $D$  is the dike depth and  $\rho_m$  is the magma density. The height above the dike center to which a column of unvesiculated magma can be raised is  $P_m(0)/\rho_m g$ , so the hydrostatic head  $C$  is

$$C = -D + \frac{D(\rho_m g - \nabla P_u) + P_o}{\rho_m g} \quad (26)$$

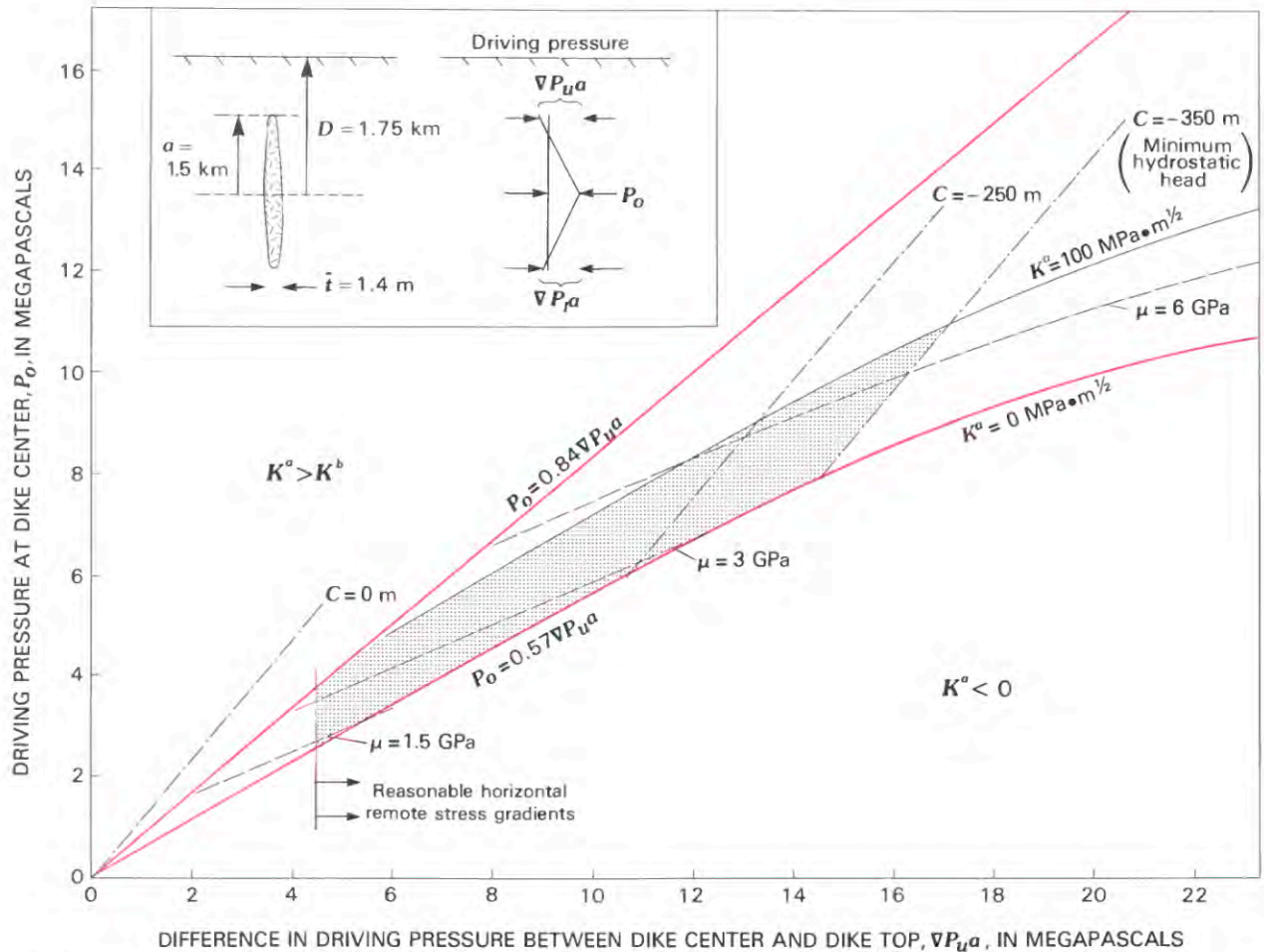


FIGURE 53.15.—Possible values of  $P_o$  and  $\nabla P_u a$  (wedge-shaped region between red lines) for the August 1981 southwest-rift-zone intrusion at Kilauea, the inferred geometry of which is shown in the inset. Values below the lower red boundary are unacceptable because  $K^a < 0$ ; values above the upper red boundary are unacceptable because values of  $K^a$  (eq 24), the hydrostatic head of the magma,  $C$  (eq 27), and the shear modulus that would result in an average dike thickness of 1.4 m (eq 23). Values within the stippled region satisfy the requirements that  $K^a < K^b$ ,  $0 < K^a < 100 \text{ MPa} \cdot \text{m}^{1/2}$ ,  $\nabla P_u \geq 3 \text{ MPa/km}$ , and  $C > -350 \text{ m}$  (see text).

Rearranging equation 26, we have

$$P_o = \frac{D}{a} \nabla P_u a + \rho_m g C. \quad (27)$$

Thus contours of the hydrostatic head are also straight lines in figure 53.15 and have a slope of  $D/a$ . For  $D/a = 1.17$  ( $a/D = 0.86$ ), any dike that has a hydrostatic head above the ground surface (to the left of contour  $C = 0$ , figure 53.15) fails to satisfy the requirement that  $K^a < K^b$ . Such a dike would grow in height (increase  $\nabla P_u a$  at constant  $P_o$  in figure 53.15), and finally erupt.

To the right of the  $C = -250 \text{ m}$  contour, the wedge-shaped region has been modified to account for the low-pressure cavity between the top of the magma and the dike tip. Instead of being

linear, contours of  $\mu$  and  $K$  deviate slightly toward lower values of  $P_o$ . Setting  $C > -350 \text{ m}$ , we find that acceptable values of  $P_o$  and  $\nabla P_u a$  are limited to below about 10.5 MPa and 17 MPa, respectively.

The lower limit on the gradient in driving pressure,  $\nabla P_u \geq 3 \text{ MPa/km}$ , becomes  $\nabla P_u a \geq 4.5 \text{ MPa}$  for  $a = 1,500 \text{ m}$ .

The stippled region in figure 53.15 contains all values of  $P_o$  and  $\nabla P_u a$  satisfying the conditions that  $K^a < K^b$ ,  $0 < K^a < 100 \text{ MPa} \cdot \text{m}^{1/2}$ ,  $C > -350 \text{ m}$ , and  $\nabla P_u \geq 3 \text{ MPa/km}$ .  $P_o$ , the excess magma pressure at the dike center, lies between about 2.5 and 10.5 MPa. The upper bound of the hydrostatic head, occurring for  $\nabla P_u a = 4.5 \text{ MPa}$  and  $P_o = 4 \text{ MPa}$ , is about 50 m beneath the surface.  $\nabla P_u a$  lies between 4.5 and 17 MPa, corresponding to

values of  $\nabla P_r$ , the difference between gradients of the magma pressure and the remote stress, of 3–11 MPa/km. This is between 1 and 4 times the difference in pressure gradients due to the density contrast between the magma and the host rock. Thus, the remote stress is bracketed by the curves shown in figures 53.14A and 53.14B. Without further refinement of the in place values of the rift-zone shear modulus and fracture toughness, it is not possible to determine these parameters more precisely. The limits of the stippled region constrain the effective shear modulus to be within a factor of 2–3 of 3 GPa. By generating diagrams such as figure 53.15 for several intrusions with different dike heights, thicknesses, and ratios of height to depth, it might be possible to constrain the shear modulus still further.

## DISCUSSION

### ASSUMPTION OF A UNIFORM FRACTURE TOUGHNESS

The assumption of a uniform fracture toughness within the rift zone requires that the remote stress and the magma pressure converge with depth over the lower half of the dike ( $\nabla P_l > 0$ ) (fig. 53.14). If  $K_c$  increases with depth, then  $\nabla P_l$  could decrease to values below those indicated. The magma-pressure and remote-stress curves could actually diverge with increasing depth, if the increase in  $K_c$  is sufficiently great and its value is much greater than laboratory values. From experimental data it appears that, in the absence of a pervasive pore fluid at a pressure equal to the confining pressure,  $K_c$  increases with depth because of increasing pressure. Although its effect is small, increasing temperature will actually decrease  $K_c$  with depth, at least to moderate temperatures. There is no evidence to support a rapid increase in  $K_c$  at pressures and temperatures corresponding to depths typical of dike bottoms.

A sequence of two dike intrusions into the southern Krafla rift zone in Iceland is instructive in this regard. The first, in September 1977, generated a swarm of earthquakes with focal depths of about 2–5 km (Brandsdottir and Einarsson, 1979), and the second, in February 1980, generated earthquakes with depths of about 4–7 km (Bryndis Brandsdottir, oral commun., 1985). On the assumption that the deeper earthquake swarm is indicative of a deeper dike, this behavior is consistent with the location of the second dike being controlled by the stress field induced by the first (fig. 53.11C). In addition it provides evidence that any increase in  $K_c$  with depth that might have stabilized the bottom of the earlier dike was not great enough to serve as a barrier to the later dike, and that the bottom of the earlier dike was well within a region capable of sustaining brittle behavior.

If some dikes on the east rift zone of Kilauea bottom within a magma conduit of high temperature and large radius of curvature, then an increase in  $K_c$  (because of microplasticity), as well as a decrease in  $K$  (because of a large radius of curvature at the dike tip) could result. Such a conduit might serve as an effective barrier to further propagation of the dike bottom.

### OTHER FACTORS THAT MIGHT INFLUENCE DIKE SHAPE

In the preceding treatment of dike stability, it was assumed that the dike had achieved an equilibrium position in the vertical plane. In the following sections we discuss factors related to magma solidification and flow which could influence dike growth and prevent the dike from reaching such an equilibrium position. Though some of these processes may warrant further study, we explain why they have been neglected in this analysis.

### MAGMA SOLIDIFICATION

Walker (1974) suggested that low wall-rock temperatures near the Earth's surface could promote magma solidification near the top of a dike and thus prevent eruption. For magma to solidify at approximately the same height as it propagates many kilometers downrift implies that very little heat loss occurs during lateral flow, compared to the heat loss that occurs during upward flow. Following the work of Delaney and Pollard (1982), we estimated the effect of host-rock temperature on the time required for magma solidification during flow in a dike. Even if upward flow occurs entirely adjacent to host rock at the low temperatures appropriate for the dike top, magma originating at a depth of 3 km has less difficulty in flowing to the surface than in flowing 10 km downrift, given a uniform dike thickness and magma flow rate. Under these circumstances, solidification should not be important in stabilizing the dike top. However, if the driving-pressure distribution is such that the dike is thinner in its upper part, and if the resulting magma velocity is less than at depth, the possibility that magma solidification occurs before the dike reaches its stable height cannot be ruled out.

The following observations of dike behavior support our contention that magma solidification, by itself, is unlikely to limit dike height: (1) Fissures that erupt generally permit magma flow to continue for several hours before solidification takes place. (2) Long-term patterns of intrusion and eruption observed at both Kilauea and Krafla (see below) are easily reconciled with evolving magma pressures and remote stresses. The alternative interpretation of this behavior as due to changing susceptibility of the magma to solidification finds no independent support. (3) At least one dike, the February 1980 intrusion into the southern Krafla rift zone, was associated with an earthquake swarm whose top was deeper than 3 km. This depth is below that at which solidification might influence propagation.

### TWO-DIMENSIONAL MAGMA FLOW

If dike growth in two dimensions is analogous to the pumping of magma at constant pressure into the base of an existing vertical slot in the Earth's crust, then lateral growth will be enhanced relative to upward growth because the pressure gradient available for upward flow is reduced by the static pressure gradient within the overlying column of magma. If this tendency is sufficiently pronounced it could

prevent dikes from reaching their equilibrium height before solidification. To estimate the significance of this effect, we compared the upward and lateral rates of one-dimensional magma flow in a slot, under the conditions of constant pressure at the origin and zero pressure at the advancing magma front. The upward flow rate is not greatly decreased relative to the lateral flow rate until the top of the magma column approaches its hydrostatic head. The hydrostatic head as a limit to the magma column height can be incorporated directly into the analysis of dike stability, as it was for the example of the August 1981 intrusion. A more complete formulation of the one-dimensional dike propagation problem than flow in an existing slot was proposed by Spence and Turcotte (1985). They assumed that the magma wets the dike walls all the way to the tip and coupled the viscous pressure loss within the magma to the elastic dilation of the dike walls. If the remote horizontal compressive stress is constant at a given depth but increases with depth at the same rate as the hydrostatic pressure in the magma column, then vertical and horizontal flow rates would be equal. Although it is not expected that the remote stress and the magma pressure increase identically with depth, the rates of increase are probably close enough that the influence of gravity on the relative vertical and horizontal magma flow rate is minimal. Therefore we feel justified in neglecting the complexities of two-dimensional magma flow in rift-zone dikes as a mechanism for preventing them from attaining their equilibrium height.

#### SUBCRITICAL CRACK GROWTH

In a chemically reactive environment, the energy required for a unit increase in crack length, and thus  $K_c$ , may be decreased. Rates of crack propagation under these conditions are controlled in part by the rate of transport of the reactive species to the crack tip and the kinetics of reaction. Anderson and Grew (1977) suggested that this process, known as subcritical crack growth, might be an important mechanism of dike propagation. However, maximum rates of subcritical crack growth in laboratory rock samples are  $10^{-2}$ – $10^{-3}$  m/s (Atkinson, 1984), about two orders of magnitude less than observed rates of rift-zone dike propagation. Moreover, these rates decrease by several orders of magnitude for small decreases in  $K$ . Therefore we have neglected this form of crack growth in our analysis. It is possible that subcritical growth occurs at the top and bottom after a dike has reached a stable height. However, the greatest distance that a typical 1-meter dike could propagate at these rates in the few hours before solidification is only about 100 m.

#### POTENTIAL APPLICATIONS OF THE MODEL

##### LONG-TERM INTRUSION/EXTRUSION BEHAVIOR

Klein (1982) noted that five of the seven dike intrusions at Kilauea within the 4 years prior to the 1975 Kalapana earthquake resulted in eruptions, whereas only two of the sixteen dike intrusions in the 6 years following the earthquake did so. The two most recent

episodes of activity at Krafla, from 1724 to 1729 and from 1975 to the present, began with a series of predominantly subsurface dikes accompanied by either minor eruptions or none, and ended with a series of fissure eruptions emitting successively increasing volumes of magma (Tryggvason, 1983; Saemundsson, 1979). This behavior is consistent with the hypothesis that large earthquakes at Kilauea (Dzurisin and others, 1980; Klein, 1982), and centuries of plate spreading in Iceland (Bjornsson and others, 1979) extend the rift zone and facilitate dike intrusion. The preceding analysis has shown that, independent of the magnitude of the remote tensile stress, a shallow dike with a hydrostatic head above the Earth's surface should erupt. Thus the magma reservoir pressure probably decreased following the 1975 Kalapana earthquake at Kilauea and increased over the course of the activity at Krafla. This conclusion is supported by the record of long-term magma reservoir inflation from 1975–1984 at Krafla (Bjornsson, 1985), and by combined geodetic and gravity data at Kilauea (Johnson, chapter 47). We emphasize that both the remote stress and the magma pressure must be considered in developing models of rift-zone dynamics.

#### IMPLICATIONS FOR MAGMA RESERVOIR BEHAVIOR

The August 1981 southwest-rift-zone intrusion at Kilauea resulted in a net summit tilt of  $-100$  mrad, about  $-50$  mrad of which occurred following the passage of the earthquake swarm beneath the geodetic level line. Using the calculation of Decker and others (1983),  $-50$  mrad corresponds to a pressure drop of about 4 MPa, which is a large percentage of the estimated maximum excess pressure of 3–11 MPa within the dike ( $P_0$  in figure 53.15). If the rift zone behaves elastically, such a decrease in  $P_0$  should be reflected by a decrease in dike thickness and possibly in dike height (if  $K^a$  drops below zero) of sufficient magnitude to be measured geodetically. Installation of a line of continuously recording deformation meters perpendicular to the rift zone might allow observations of these changes, which in turn could be used to estimate the change in reservoir pressure.

#### ALONG-STRIKE VARIATION OF DIKE GEOMETRY

In addition to magma pressure variation with time, the magma pressure at a given depth within a dike increases with downrift distance because of the slope of the rift zones, and decreases with downrift distance because of viscous pressure loss. The balance between these two factors might be reflected in the locations of fissure eruptions, and in along-strike variations in dike height and thickness that could be measured geodetically. These observations might be useful in further constraining the remote stress field, because the sensitivity of the dike thickness and height to changes in magma pressure are dependent upon the gradient in the driving pressure (fig. 53.16). For example, a dike is more likely to maintain a fairly constant thickness and height for tens of kilometers if the gradients of

the superimposed remote tensile stress acting on the rift zone are large, as in figure 53.16B. Thus, it seems likely that data constraining temporal and spatial variations in dike geometry could significantly enhance our understanding of rift-zone dynamics.

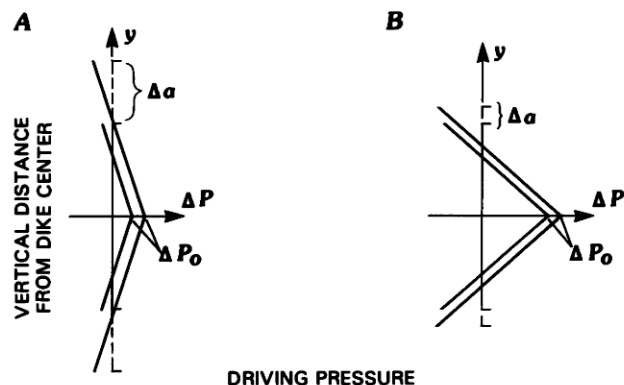


FIGURE 53.16.—Schematic diagrams illustrating the change in dike half-height for a given change in magma pressure.  $K_c$  is taken to be zero. **A**,  $P_o = 3$  MPa; **B**,  $P_o = 11$  MPa. For a 2-MPa increase in magma pressure  $\Delta P_o$ , the dike in **A** increases in half-height by a factor of 1.67; that in **B** increases by a factor of only 1.18. The dike thicknesses increase as the square of these factors, or by factors of 2.8 and 1.4, respectively.

## REFERENCES CITED

- Anderson, E.M., 1938, The dynamics of sheet intrusion: Royal Society of Edinburgh Proceedings, Series B, v. 58, p. 242-251.
- Anderson, O.L., and Grew, P.C., 1977, Stress corrosion theory of crack propagation with application to geophysics: *Review of Geophysics and Space Physics*, v. 15, p. 77-104.
- Atkinson, B.K., 1984, Subcritical crack growth in geologic materials: *Journal of Geophysical Research*, v. 89, p. 4077-4114.
- Bieniawski, Z.T., 1978, Determining rock mass deformability: experience from case histories [abs.]: *International Journal of Rock Mechanics, Mineral Science and Geomechanics, Abstracts*, v. 15, p. 237-247.
- Birch, F., 1966, Compressibility; elastic constants, in *Handbook of Physical Constants: Geological Society of America Memoir 97*, p. 97-173.
- Bird, R.B., Stewart, W.E., and Lightfoot, E.N., 1960, *Transport phenomena*: New York, John Wiley & Sons, 780 p.
- Bjornsson, A., 1985, Dynamics of crustal rifting in NE Iceland: *Journal of Geophysical Research*, v. 90, p. 10,151-10,162.
- Bjornsson, A., Johnsen, G., Sigurdsson, S., Thorbergsson, G., and Tryggvason, E., 1979, Rifting of the plate boundary in north Iceland 1975-1978: *Journal of Geophysical Research*, v. 84, p. 3029-3038.
- Brandsdottir, B., and Einarsson, P., 1979, Seismic activity associated with the September 1977 deflation of Krafla Volcano in north-eastern Iceland: *Journal of Volcanology and Geothermal Research*, v. 6, p. 197-212.
- Broek, D., 1982, *Elementary Engineering Fracture Mechanics*: Boston, Martinus Nijhoff Publishers, 469 p.
- Broyles, M.L., Suyenaga, W., and Furumoto, A.S., 1979, Structure of the lower east rift zone of Kilauea Volcano, Hawaii, from seismic and gravity data: *Journal of Volcanology and Geothermal Research*, v. 5, p. 317-336.
- Davis, P.M., 1976, The computed piezomagnetic anomaly field for Kilauea Volcano, Hawaii: *Journal of Geomagnetism and Geoelectricity*, v. 28, p. 113-122.
- Decker, R.W., Okamura, A.T., and Dvorak, J.G., 1983, Pressure changes in the magma reservoir beneath Kilauea Volcano, Hawaii: *Eos (American Geophysical Union Transactions)*, v. 64, p. 901.
- Delaney, P., and Pollard, D.D., 1981, Deformation of host rocks and flow of magma during growth of minette dikes and breccia-bearing intrusions near Ship Rock, New Mexico: U.S. Geological Survey Professional Paper 1202, 61 p.
- 1982, Solidification of basaltic magma during flow in a dike: *American Journal of Science*, v. 282, p. 856-885.
- Delaney, P.T., Pollard, D.D., Ziony, J.I., and McKee, E.H., in press, Field relations between dikes and joints: emplacement processes and paleostress analysis: *Journal of Geophysical Research*.
- Dzurisin, D., Anderson, L.A., Eaton, G.P., Koyanagi, R.Y., Lipman, P.W., Lockwood, J.P., Okamura, R.T., Puniwai, G.S., Sako, M.K., and Yamashita, K.M., 1980, Geophysical observations of Kilauea Volcano, Hawaii, 2. Constraints on the magma supply during November 1975-September 1977: *Journal of Volcanology and Geothermal Research*, v. 7, p. 241-269.
- Einarsson, P., and Brandsdottir, B., 1979, Seismological evidence for lateral magma intrusion during the July 1978 deflation of the Krafla Volcano in NE-Iceland: *Journal of Geophysics*, v. 47, p. 160-165.
- Epp, D., Decker, R.W., and Okamura, A.T., 1983, Relation of summit deformation to east rift zone eruptions on Kilauea Volcano, Hawaii: *Geophysical Research Letters*, v. 10, p. 493-496.
- Evans, K., 1982, Some examples and implications of observed elastic deformations associated with the growth of hydraulic fractures in the Earth, in Zoback, M.D., and Haimson, B.C., eds., *Proceedings of Workshop XVII, Hydraulic Fracturing Stress Measurements*, U.S. Geological Survey Open-File Report 82-1075, v. 2, p. 661-698.
- Fiske, R.S., and Jackson, D.E., 1972, Orientation and growth of Hawaiian volcanic rifts: the effect of regional structure and gravitational stress: *Proceedings of the Royal Society of London, Series A*, v. 329, p. 299-326.
- Fujii, T., and Kushiro, I., 1977, Density, viscosity, and compressibility of basaltic liquid at high pressures: *Carnegie Institution of Washington Yearbook*, 1976, p. 419-424.
- Hauksson, E., 1983, Episodic rifting and volcanism at Krafla in north Iceland: growth of large ground fissures along the plate boundary: *Journal of Geophysical Research*, v. 88, p. 626-636.
- Helgason, J., and Zentilli, M., 1985, Field characteristics of laterally emplaced dikes: anatomy of an exhumed Miocene dike swarm in Reydarfjörður, eastern Iceland: *Tectonophysics*, v. 115, p. 247-274.
- Hoffman, J.P., Ulrich, G.E., and Chadwick, W.W., 1984, Geodetic measurements on the East Rift Zone, Kilauea Volcano, Hawaii: *Eos (American Geophysical Union Transactions)*, p. 1131.
- Kinoshita, W.T., Krivoy, H.L., Mabey, D.R., and MacDonald, R.R., 1963, Gravity survey of the Island of Hawaii: U. S. Geological Survey Professional Paper 475-C, p. C114-C116.
- Klein, F.W., 1982, Patterns of historical eruptions at Hawaiian volcanoes: *Journal of Volcanology and Geothermal Research*, v. 12, p. 1-35.
- Lawn, B.R., and Wilshaw, T.R., 1975, *Fracture of brittle solids*: Cambridge, Cambridge University Press, 204 p.
- Macdonald, G.A., 1956, The structure of Hawaiian volcanoes: *Verhandelingen van het Koninklijke Nederlandsch-Geologisch-Mijnbouwkundig Genootschap*, v. 16, p. 274-295.
- McTigue, D.F., and Mei, C.C., 1981, Gravity-induced stresses near topography of small slope: *Journal of Geophysical Research*, v. 86, p. 9268-9278.
- Meredith, P.G., and Atkinson, B.K., 1985, Fracture toughness and subcritical crack growth during high-temperature tensile deformation of Westerly granite and Black gabbro: *Physics of the Earth and Planetary Interiors*, v. 39, p. 33-51.
- Moore, J.G., and Fiske, R.S., 1969, Volcanic substructure inferred from dredge samples and ocean-bottom photographs, Hawaii: *Geological Society of America Bulletin*, v. 80, p. 1191-1202.
- Palmason, G., 1971, Crustal Structure of Iceland from explosion seismology: *Societas Scientiarum Islandica, publ. 40*, 187 p.

- Paris, P.C., and Sih, G.C., 1965, Stress analysis of cracks, fracture toughness testing and its applications, Philadelphia, ASTM, p. 30-81.
- Pollard, D.D., 1976, On the form and stability of open hydraulic fractures in the Earth's crust: *Geophysical Research Letters*, v. 3, p. 513-516.
- Pollard, D.D., Delaney, P.T., Duffield, W.A., Endo, E.T., and Okamura, A.T., 1983, Surface deformation in volcanic rift zones: *Tectonophysics*, v. 94, p. 541-584.
- Pollard, D.D., and Holzhausen, G., 1979, On the mechanical interaction between a fluid-filled crack and the Earth's surface: *Tectonophysics*, v. 53, p. 27-57.
- Pollard, D.D., and Segall, P., in press, Theoretical displacements and stresses near fractures in rocks: with applications to faults, joints, veins, dikes, and solution surfaces, in Atkinson, B. K., ed., *Rock fracture mechanics*: London, Academic Press.
- Ryan, M.P., Blevins, J.Y.K., Okamura, A.T., and Koyanagi, R.Y., 1983, Magma reservoir subsidence mechanics: theoretical summary and application to Kilauea Volcano, Hawaii: *Journal of Geophysical Research*, v. 88, p. 4147-4181.
- Ryan, M.P., Koyanagi, R.Y., and Fiske, R.S., 1981, Modeling the three-dimensional structure of macroscopic magma transport systems: application to Kilauea Volcano, Hawaii: *Journal of Geophysical Research*, v. 86, p. 7111-7129.
- Saemundsson, K., 1979, Outline of the geology of Iceland: *Jokull*, v. 29, p. 7-28.
- Schmidt, R.A., and Huddle, C.W., 1977, Effect of confining pressure on fracture toughness of Indiana limestone [abs.]: *International Journal of Rock Mechanics and Mining Sciences & Geomechanics Abstracts*, v. 14, p. 289-293.
- Secor, D.T., and Pollard, D.D., 1975, On the stability of open hydraulic fractures in the Earth's crust: *Geophysical Research Letters*, v. 2, p. 510-513.
- Shah, R.C., and Kobayashi, A.S., 1973, Stress-intensity factors for an elliptical crack approaching the surface of a semi-infinite solid: *International Journal of Fracture*, v. 9, p. 3-21.
- Sigurdsson, H., and Sparks, S.R.J., 1978, Lateral flow within rifted Icelandic crust: *Nature*, v. 274, p. 126-130.
- Spence, D.A., and Turcotte, D.L., 1985, Magma-driven propagation of cracks: *Journal of Geophysical Research*, ser. B, v. 90, no. 1, p. 575-580.
- Swanson, D.A., Duffield, W.A., and Fiske, R.S., 1976, Displacement of the south flank of Kilauea Volcano: the result of forceful intrusion of magma into rift zones: U.S. Geological Survey Professional Paper 963, 39 p.
- Tada, H., Paris, P.C., and Irwin, G.R., 1973, *The stress analysis of cracks handbook*: Hellertown, Pa., Del Research Corp.
- Tryggvason, E., 1983, The widening of the Krafla fissure swarm during the 1975-1981 volcano-tectonic episode: *Nordic Volcanological Institute Report* 8304, 48 p.
- Walker, G.P.L., 1959, Geology of the Reydarfjordur area, eastern Iceland: *Quarterly Journal of the Geological Society of London*, v. 114, p. 367-393.
- , 1963, The Breiddalur central volcano, eastern Iceland: *Quarterly Journal of the Geological Society of London*, v. 119, p. 23-63.
- , 1974, Eruptive mechanisms in Iceland, in Krisjansson, ed., *Geodynamics of Iceland and the North Atlantic area*: Dordrecht-Holland, D. Reidel, p. 189-201.
- Weertman, J., 1971, Theory of water-filled crevasses in glaciers applied to vertical magma transport beneath oceanic ridges: *Journal of Geophysical Research*, v. 76, p. 1171-1183.
- Williams, H., and McBirney, A.R., 1979, *Volcanology*: San Francisco, Freeman, Cooper, 397 p.
- Winter, R.B., 1983, *Bruchmechanische Gerteinsuntersuchungen mit dem Bezug zu Hydraulischen Frac-Versuchen in Tiefbohrungen*: Bochum, Ruhr-Universität, Institut für Geophysik, Ph. D. dissertation.
- Zucca, J.J., Hill, D.P., and Kovach, R.L., 1982, Crustal structure of Mauna Loa Volcano, Hawaii, from seismic refraction and gravity data: *Bulletin of the Seismological Society of America*, v. 72, p. 1535-1550.